



Frequency-Sensitivity and Magnitude-Sensitivity in Decision-Making: Predictions of a Theoretical Model-Based Study

Thomas Bose¹ · Freya Bottom² · Andreagiovanni Reina¹ · James A. R. Marshall¹

© The Author(s) 2019

Abstract

We theoretically study decision-making behaviour in a model-based analysis related to binary choices with pulsed stimuli. Assuming a strong coupling between external stimulus and its internal representation, we argue that the frequency of external periodic stimuli represents an important degree of freedom in decision-making which may modulate behavioural responses. We consider various different stimulus conditions, including varying overall magnitudes and magnitude ratios as well as varying overall frequencies and frequency ratios, and different duty cycles of the pulsed stimuli. Decision time distributions, mean decision times and choice probabilities are simulated and compared for two different models—a leaky competing accumulator model and a diffusion-type model with multiplicative noise. Our results reveal an interplay between the sensitivity of the model systems to both frequency and magnitude of the stimuli. In particular, we find that periodic stimuli may shape the decision time distributions resulting from both models by resembling the frequencies of the pulsed stimuli. We obtain significant frequency-sensitive effects on mean decision time and choice probability for a range of overall frequencies and frequency ratios. Our simulation analysis makes testable predictions that frequencies comparable with typical sensory processing and decision-making timescales may influence choice and response times in perceptual decisions. A possible experimental implementation is proposed.

Keywords Binary decision-making · Behaviour · Computational modelling · Pulsed stimuli · Response times

Introduction

When the brain makes decisions, it accumulates evidence to compute a decision variable that is evaluated against a decision criterion (Gold and Shadlen 2007). This concept has been tested and verified in binary decision-making tasks in a variety of different settings: from perceptual decision-making (Shadlen and Newsome 1996, 2001; Usher and McClelland 2001; Ditterich et al. 2003; Bogacz et al. 2006; Pirrone et al. 2018) to value-based decisions (Krajbich et al. 2010, 2015; Basten et al. 2010; Hunt et al. 2012; Pirrone et al. 2018), and choice behaviour when value and sensory evidence are integrated together (Feng et al. 2009; Afacan-Seref et al. 2018).

In perceptual decision-making, the computation of the log-likelihood ratio between the probabilities of evidence

(given two alternative hypotheses) to decide in favour of one of the two available options is related to the optimal way to trade-off between speed and accuracy, i.e. given a certain required accuracy, the decision time is minimised (Bogacz et al. 2006; Gold and Shadlen 2007). The sequential accumulation of multiple pieces of evidence until a stop-and-decide criterion is fulfilled can be realised by the sequential probability ratio test (SPRT) (Wald and Wolfowitz 1948). Making the transition from discrete to continuous time, it has been shown that the drift-diffusion model (DDM) (Ratcliff 1978; Ratcliff et al. 2016) resembles the SPRT, where the decision variable in the DDM directly relates to the sum of likelihood ratios computed consecutively over discrete timesteps in the SPRT (Bogacz et al. 2006). Potential similarities between key factors in perceptual decisions and value-based choices have been noted (e.g. see (Sugrue et al. 2005; Gold and Shadlen 2007; Polanía et al. 2014; Tajima et al. 2016; Pirrone et al. 2018)). In particular, it has been shown that difference-based accumulation of evidence is fundamental not only in perceptual but also in value-based decisions (Basten et al. 2010, but see Pirrone et al. 2014).

Magnitude-sensitivity has emerged as a key feature in perceptual decision-making (Pins and Bonnet 1996;

✉ Thomas Bose
t.bose@sheffield.ac.uk

¹ Department of Computer Science, University of Sheffield, Sheffield, UK

² Department of Physics, University of Sheffield, Sheffield, UK

Stafford and Gurney 2004; Palmer et al. 2005; Teodorescu et al. 2016; Pirrone et al. 2018; Polanía et al. 2014; Ratcliff et al. 2018; van Maanen et al. 2012) and in economic choices (Hunt et al. 2012; Pirrone et al. 2014, 2018; Polanía et al. 2014). This is characterised by decreasing decision times for both increasing magnitude (value) differences and increasing overall magnitudes (values) (Pins and Bonnet 1996; Stafford and Gurney 2004; Palmer et al. 2005; Hunt et al. 2012; Teodorescu et al. 2016; Polanía et al. 2014; Pirrone et al. 2014, 2018; Ratcliff et al. 2018; van Maanen et al. 2012). Furthermore, this hallmark is also proposed to be present in collective decision-making of social insects. For example, sensitivity to the quality of nest-sites in the decision-making of house-hunting honeybees has been found in mathematical analyses (Pais et al. 2013; Reina et al. 2017; Reina et al. 2018) and has been discussed theoretically (Pirrone et al. 2014; Bose et al. 2017).

When external stimuli enter the brain, they undergo a transformation into corresponding internal representations (Gold and Shadlen 2007). In recent brightness discrimination experiments and modelling studies, it has been shown that assuming a strong coupling between external stimulus and internal model dynamics could explain empirical data (Teodorescu et al. 2016; Ratcliff et al. 2018). Both studies focused on magnitude-sensitive effects where two visual stimuli were sampled from Gaussian distributions centred at a mean brightness (Teodorescu et al. 2016; Ratcliff et al. 2018). That is, the brightnesses of both stimuli were allowed to vary randomly within a trial at a refresh rate of 60 Hz. However, pulsed stimuli with well-defined frequencies (i.e. clearly distinguishable low-magnitude and high-magnitude phases) have not yet been studied in such a scenario where external stimulus and internal variable may be assumed to be strongly coupled. Given a strong direct coupling of this type (see Eq. 2 below), we hypothesised that the stimulus frequency, in addition to the stimulus magnitude, could be another degree of freedom that influences decision-making behaviour. To investigate this hypothesis and to see what effects varying stimulus frequencies might induce, we simulated a brightness discrimination experiment similar to the ones previously studied by Teodorescu et al. (2016) and Ratcliff et al. (2018), and analysed possible behavioural responses employing sequential sampling models. We applied a DDM with *multiplicative* noise (denoted mDDM in the following), where the input signal directly enters the coefficient determining the noise strength (Brunton et al. 2013; Teodorescu et al. 2016). Here, we included multiplicative noise, as it has been shown that this modification of the canonical DDM gives a better account for the magnitude-sensitive decision task we simulate in the present paper (Teodorescu et al. 2016; Ratcliff et al. 2018). We compared results obtained from the mDDM variant with those from a leaky competing accumulator (LCA)

model (Usher and McClelland 2001), which has also been shown to account for magnitude-sensitive data (Teodorescu et al. 2016; Ratcliff et al. 2018), and, as a new aspect, here, we analysed how both models perform under variation of overall frequency and frequency ratio of the two stimuli presented periodically. In particular, our analysis of the simulated behavioural data shows that, in addition to sensitivity to the overall magnitude and the magnitude ratio of the two stimuli, the computation of the decision variable also exhibits sensitivity to the stimuli's overall frequency and frequency ratio. Our results demonstrate that, under the assumption of a strong coupling between external and internal stimulus, the LCA model and mDDM are both magnitude-sensitive and frequency-sensitive, and qualitatively show largely similar behaviour. In particular, our analysis indicates that the stimulus frequency may shape the simulated decision time distribution by transferring the periodicity of the input signal to the behavioural response. Furthermore, we identify the numerical ranges where strong frequency-sensitive effects are observed, given our particular model assumptions and propose a possible experimental implementation to test our predictions.

Materials and Methods

In this study, we assumed that the decision-making process is described by the temporal evolution of activity levels of a decision variable governed by the LCA model and the mDDM, respectively. In particular, we simulated the evolution of the decision variable for both models until a threshold, i.e. z_{LCA} or z_{mDDM} , was reached. If the threshold criterion was not met within the maximum time $t_{\text{max}} = 15$ s, we excluded the result. However, indecision was generally a rare event and in the majority of parameter combinations, we achieved an exclusion rate which was far below 1% or equal to zero. Only for low signal magnitudes, we occasionally observed slightly higher exclusion rates which however never exceeded 2%. In all simulations, we used a Euler method with a timestep of $dt = 0.001$ in the numerical integration, which gave a good compromise between computation time and accuracy. In what follows, we consider the employed stimulus conditions and both models (mDDM and LCA) in more detail.

Input Signal and Stimulus Conditions We modelled the input signals using periodic square wave functions S_j , $j = 1, 2$, which have the following form

$$S_j(t) = m_j s_j(2\pi f_j t), \quad j = 1, 2$$

$$s_j = \begin{cases} 1, & \text{if } \frac{n}{f_j} \leq t \leq \frac{n+DC_j}{f_j} \\ \frac{0.2}{m_j}, & \text{otherwise} \end{cases}, \quad n = 0, 1, 2, 3, \dots, \quad (1)$$

where t is the time and n is a positive integer used to discriminate between high-magnitude and low-magnitude intervals of the stimulus. Frequencies and magnitudes of the two stimuli are denoted, f_j and m_j , respectively. The DC_j represent the duty cycles of the signals S_j and are further explained below. Here, we assume that for both $S_1(t)$ and $S_2(t)$, there is always a baseline signal present to provide well-defined input signals (Teodorescu et al. 2016; Pirrone et al. 2018).

The signal in Eq. 1 is purely deterministic. To account for a more realistic stimulus, we add a small, normally distributed random number to the signal, i.e. $\tilde{S}_j = S_j + \mathcal{N}(\text{mean} = 0, \text{SD} = 0.05)$ at each timestep. This stochastic signal is then transformed into an internal representation of the input, $I_j(t)$, according to

$$I_j(t) = \tilde{S}_j^\gamma(t), \tag{2}$$

where γ is an exponent characterising the nonlinear relationship between \tilde{S}_j and I_j . Again and for the same reasons as discussed before for the stimulus signal S_j , we assume a lower threshold for the transformed signal I_j , i.e. at each point in time we use $I_j \leftarrow \max(0.1, I_j)$. The transformation rule in Eq. 2 was considered previously by Teodorescu et al. (2016) and was shown to provide reasonable fits to data. The authors found values of γ for various models roughly between 0.2 and 0.8 (Teodorescu et al. 2016). γ values in the LCA model employed in the study by Teodorescu et al. (2016) had an average close to 0.3 and the mDDM model studied there had a mean value near 0.7 (Teodorescu et al. 2016). In our study, we used a fixed value of $\gamma = 0.5$, which is well within the range observed by Teodorescu et al. (2016) and should hence be appropriate for our modelling purposes. Another reason for choosing the same γ for both models is that the transformation rule in Eq. 2 does not depend on the choice of the model to compute the decision variable and may therefore be the same for both mDDM and LCA model.

Besides altering magnitudes and frequencies of the input signals, we also modified the duty cycle (DC) of the input signals in Eq. 1, which, in our terms, quantifies the time the signal is at its maximum value in relation to a reference time unit. Specifically, we considered the case where the duty cycles of both signals are 50%, i.e. $DC_1 = 0.5 = DC_2$. We denote this stimulus condition SC1. In addition, we investigate stimulus condition SC2, where $DC_2 = 0.5$ and $DC_1 = DC_2 f_1/f_2$, that is the duty cycle of signal 1 is proportional to the ratio of the frequencies of both signals. Condition SC2 is useful, as it allows to vary frequencies and duty cycle simultaneously. In both stimulus conditions, pulse widths are inversely proportional to the signal frequencies. Duty cycles and pulse widths of both signals are equal if $f_1 = f_2$. However, the difference between stimulus conditions SC1 and SC2 is that in condition SC2, the pulse

width of S_1 is smaller (bigger) than the pulse width of S_2 if $f_1 < f_2$ ($f_1 > f_2$). In condition SC1, the inverse applies, as the duty cycle is kept constant at 50%. The different stimulus conditions are summarised in Table 1 and illustrated in the two upper panels in Fig. 1a and b, respectively.

Implementation of the mDDM Model The first model we study is the mDDM, i.e. a diffusion-type model with multiplicative noise (Brunton et al. 2013; Teodorescu et al. 2016), which is implemented according to

$$dx(t) = q(I_1(t) - I_2(t))dt + \Gamma(I_1, I_2)dW(t), \tag{3}$$

where x represents the decision variable. I_1 and I_2 are the transformed inputs introduced in Eq. 2, q is a transformation rate, and dW is the increment of a Wiener process, which is normally distributed, i.e. $dW \sim \mathcal{N}(\text{mean} = 0, \text{SD} = 1)$. The Wiener process is included to model noise in the decision-making process. $\Gamma(I_1, I_2)$ is an input-dependent coefficient of the noise term and has the form (Teodorescu et al. 2016)

$$\Gamma(I_1, I_2) = \sqrt{\sigma_{\text{mDDM}}^2 + \Phi(I_1^2 + I_2^2)}, \tag{4}$$

where σ_{mDDM} characterises a constant processing noise in the decision variable $x(t)$ and Φ quantifies the strength of the multiplicative noise originating from the transformed input signals.

Furthermore, we assume that the internal representation of the drift term in Eq. 3, i.e. $q(I_1(t) - I_2(t))$, underlies trial-to-trial variability. This means that we add a small, Gaussian random number sampled from $\mathcal{N}(\text{mean} = 0, \text{SD} = 0.1)$ to this term at the beginning of each trial. We also take into account that the initial condition is not perfectly symmetric by assuming a starting point variability (SPV) of 0.1 across trials, and sample the starting value $x(t = 0)$ from a uniform distribution $\mathcal{U}(-\text{SPV}, \text{SPV})$. The inclusion of across-trial variability in drift rate and starting point values in diffusion models have been shown to better explain behavioural data (e.g. see Ratcliff and Rouder (1998) and Ratcliff and Tuerlinckx (2002)).

Implementation of the LCA Model The second model we apply in this paper is a mutual inhibition model, originally introduced as the leaky competing accumulator model

Table 1 Overview of stimulus conditions

Stimulus condition	Input $I_1(t)$	Input $I_2(t)$
SC1	$DC_1 = 0.5$	$DC_2 = 0.5$
SC2	$DC_1 = f_1/(2 f_2)$	$DC_2 = 0.5$

DC denotes the duty cycle of the signal and is given as a ratio. A duty cycle of 50% (i.e. $DC = 0.5$), for example, means in our terms that a signal is at its maximum 50% of the time

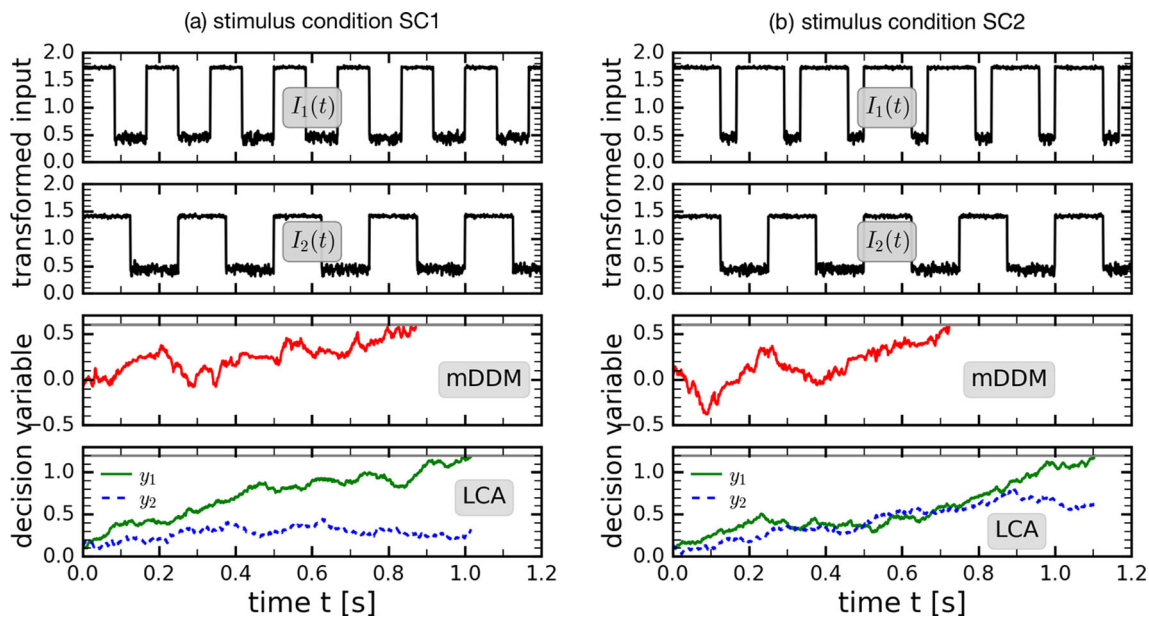


Fig. 1 Simulations of the two different models (mDDM and LCA) for two different stimulus conditions (cf. Table 1). The models are integrated until the threshold is reached. We used $f_1 = 6\text{Hz}$, $f_2 = 4\text{Hz}$, $m_1 = 3$, $m_2 = 2$ in the numerical integration

(Usher and McClelland 2001). In mathematical terms, this is expressed as

$$\begin{aligned}
 dy_1(t) &= (-k y_1(t) - \beta y_2(t) + q I_1(t)) dt \\
 &\quad + \sigma_{\text{LCA}} dW_1(t), \\
 dy_2(t) &= (-k y_2(t) - \beta y_1(t) + q I_2(t)) dt \\
 &\quad + \sigma_{\text{LCA}} dW_2(t),
 \end{aligned}
 \tag{5}$$

where y_1 and y_2 describe the activity levels of the evidence-integrating units, i.e. a decision variable comprised of two elements. If either of the two integrators crosses a given threshold, a decision is made. Again, q is the transfer rate that scales original stimulus and internal representation of that input, and I_1 and I_2 are the transformed input signals according to Eq. 2. The activity level of each accumulator is independently affected by fluctuations modelled by Wiener processes with increments dW_1 and dW_2 and quantified by σ_{LCA} , where we again have $dW_j \sim \mathcal{N}(\text{mean} = 0, \text{SD} = 1)$. Information loss in the accumulators is characterised by the leak rate k . Cross-inhibition is included by the terms $\propto \beta$, where β denotes the inhibition strength. Models featuring cross-inhibition have been studied frequently in two alternative choice tasks both in nonlinear (Usher and McClelland 2001; Brown and Holmes 2001; Brown et al. 2005; Wong and Wang 2006; Bogacz et al. 2007) and linear versions (Bogacz et al. 2006; Marshall et al. 2015; Teodorescu et al. 2016). Furthermore, it has been shown previously that competitive models like the LCA account better for magnitude-sensitive data compared with non-competitive models (Teodorescu and Usher 2013). As in the mDDM, in the LCA model in Eq. 5, we also take into

account starting point variability ($\text{SPV} = 0.2$) across trials and sample initial conditions from uniform distributions, i.e. $y_j(t = 0) \sim \mathcal{U}(0, \text{SPV})$, $j = 1, 2$.

Model Parameters The following parameters are fixed throughout the paper: $k = 0.5$, $\beta = 0.25$, $q = 1$, $\gamma = 0.5$, $\Phi = 0.1$, $\sigma_{\text{LCA}} = 0.3$, $\sigma_{\text{mDDM}} = 0.1$, $z_{\text{LCA}} = 1.2$ and $|z_{\text{mDDM}}| = 0.6$. Frequencies $f_{1,2}$ and magnitudes $m_{1,2}$ are varied. For the following analysis, we introduce the magnitude ratio as $\rho_m = m_1/m_2$, the overall magnitude as $\Upsilon_m = m_1 + m_2$ and the magnitude difference as $\Delta_m = |m_1 - m_2|$. In the same way, we define the frequency ratio of the two stimuli as $\rho_f = f_1/f_2$, the overall frequency as $\Upsilon_f = f_1 + f_2$ and the frequency difference according to $\Delta_f = |f_1 - f_2|$. The relations between ρ_m (ρ_f), Υ_m (Υ_f) and Δ_m (Δ_f) are summarised in Table 2. In our theoretical study, we were particularly interested in frequencies that are well below the stimulus refresh rate used in the related experiment ($\sim 60\text{Hz}$ in Teodorescu et al. 2016) to

Table 2 Overview of the relations between magnitude (frequency) ratio, magnitude (frequency) difference and overall magnitude (frequency)

Magnitude/frequency	Expression
Of stimulus j :	m_j, f_j
Overall value:	$\Upsilon_m = m_1 + m_2, \Upsilon_f = f_1 + f_2$
Ratio:	$\rho_m = \frac{m_1}{m_2}, \rho_f = \frac{f_1}{f_2}$
Difference:	$\Delta_m = m_1 - m_2 = \Upsilon_m \left \frac{\rho_m - 1}{\rho_m + 1} \right $ $\Delta_f = f_1 - f_2 = \Upsilon_f \left \frac{\rho_f - 1}{\rho_f + 1} \right $

discriminate effects of stimulus frequency from flickering due to re-sampling of the external stimulus. Furthermore, the frequencies used in our study ($f_{1,2} \sim 0.5 - 10$ Hz), correspond to timescales in the range of 100 ms – 2 s. This interval includes the typical range for sensory processing involved in cognitive tasks such as motion discrimination and speech recognition (~ 100 ms) (Mauk and Buonomano 2004; Kiebel et al. 2008) but also typical decision times ~ 1 s obtained under laboratory conditions (e.g. see Ratcliff et al. 2016, and references therein).

Results

Performance Under Stimuli with Constant Magnitude

To get an overview of the performance of the mDDM and the LCA model and to enable better comparability with periodic stimuli, we first studied both models when the stimulus magnitude is constant and not pulsed. In Fig. 2, we show decision time distributions for varying overall magnitudes with constant magnitude ratios (Fig. 2a–d) and varying magnitude ratios with constant overall magnitudes (Fig. 2e–h). A comparison of mDDM and LCA in Fig. 2 demonstrates that both models exhibit similar qualitative

behaviour. For increasing Υ_m and constant ρ_m , the peak of the decision time distribution moves towards smaller decision times and the distribution becomes narrower (Fig. 2a–d). In contrast, for increasing ρ_m and constant Υ_m , decision time distributions of both models do not show such a significant effect (Fig. 2e–h). We also note that the shape of the distribution for both models depends on the parameter set chosen. In fact, parameters can be altered such that the decision time distributions of both models appear more similar. For example, it was shown that both models the LCA and the mDDM could be used to fit the same set of magnitude-sensitive data (Teodorescu et al. 2016). This, however, meant that γ values obtained from the fitting were different for mDDM and LCA (Teodorescu et al. 2016). Here, we applied a different approach by using the same γ value for LCA and mDDM, following our assumption that signal pre-processing is the same for both models. Other important model parameters are the multiplicative noise strength, Φ , in the mDDM and the cross-inhibition strength, β , in the LCA. Those parameters have fixed values in our study but we would expect some changes in the decision time distribution when modifying the values of these parameters, such as a shift of the peak and a variation of the distribution width. Furthermore, in case of $\Phi = 0$, the mDDM would reduce to a model similar to the standard DDM which could not fit related

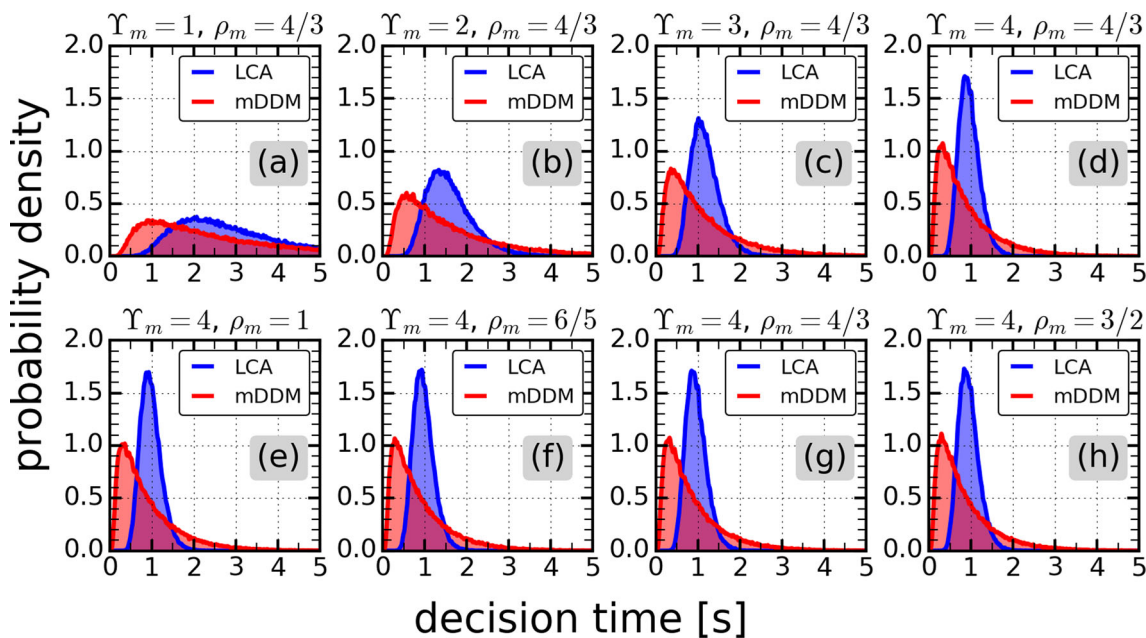


Fig. 2 Decision time distribution for continuous constant stimuli, keeping either $\rho_m = 4/3 = \text{const.}$ **a–d** or $\Upsilon_m = 4 = \text{const.}$ **e–f**. **a:** $\Upsilon_m = 1$ ($m_1 \approx 0.57, m_2 \approx 0.43$); **b:** $\Upsilon_m = 2$ ($m_1 \approx 1.14, m_2 \approx 0.86$); **c:** $\Upsilon_m = 3$ ($m_1 \approx 1.71, m_2 \approx 1.29$); **d:** $\Upsilon_m = 4$ ($m_1 \approx 2.29, m_2 \approx 1.71$); **e:** $\rho_m = 1$ ($m_1 \approx 2.0, m_2 \approx 2.0$); **f:** $\rho_m = 6/5$ ($m_1 \approx 2.18, m_2 \approx 1.82$); **g:** $\rho_m = 4/3$ ($m_1 \approx 2.29, m_2 \approx 1.71$); **h:** $\rho_m = 3/2$ ($m_1 \approx 2.4, m_2 \approx 1.6$). Each distribution is based on

the simulation of 10^5 trials of the LCA model (5) and the mDDM (Eqs. 3 and 4). Distributions shown are normalised histograms, where the coloured area under the curve equals 1. The bin-width is narrow ($0.025 \hat{=} 200$ bins for the decision time interval shown). The curve superposing the histogram goes through the centers of the bins and is interpolated in between

magnitude-sensitive empirical data (Teodorescu et al. 2016; Ratcliff et al. 2018). Considering the LCA, in case of $\beta = 0$, both accumulators would not interact in which case the model would approximate an uncoupled race model. In empirical studies, nonzero lateral inhibition has been found to be a crucial model component to account for magnitude-sensitive effects (Teodorescu et al. 2016).

In Fig. 3, we depict mean decision times, $\langle DT \rangle$, and the probabilities of choosing option 1, $\text{Pr}(\text{opt1})$, that correspond to the distributions in Fig. 2. This further underlines the sensitivity of the LCA and mDDM to varying overall magnitudes and varying magnitude ratios. In particular, we can see that $\langle DT \rangle$ decreases for both increasing overall magnitudes (Fig. 3a) as well as increasing magnitude ratios Fig. 3b, although the effect of the latter is not as strong as that of the former, which is in agreement with Fig. 2. However, if we inspect the behaviour of $\text{Pr}(\text{opt1})$, we recognise that $\text{Pr}(\text{opt1})$ increases with increasing Υ_m for the LCA model, whereas $\text{Pr}(\text{opt1})$ decreases with increasing Υ_m for the mDDM (Fig. 3a). The behaviour observed for the mDDM is a consequence of the multiplicative noise, which may cause the decision variable meet the decision threshold faster while at the same time the increase of noise also reduces accuracy. This qualitatively different behaviour of LCA and mDDM is not present in Fig. 3b, where $\text{Pr}(\text{opt1})$ increases with increasing ρ_m for both models. Furthermore, correctly, we find that for $\rho_m = 1$, i.e. in case of two stimuli with equal magnitudes, option 1 is chosen in 50% of all trials (Fig. 3b).

We point out that increasing Υ_m and keeping ρ_m constant as well as increasing ρ_m and keeping Υ_m constant increase the magnitude difference Δ_m (see Table 2). Therefore, our results are in qualitative agreement with findings reported by Hunt et al. (2012), Polanía et al. (2014), Pais et al. (2013), Reina et al. (2018), Ratcliff et al. (2018), Pirrone et al. (2014, 2018) and van Maanen et al. (2012). A negative correlation between input magnitude and decision time is reminiscent of Piéron’s law according to which higher stimulus magnitudes lead to faster decisions (e.g. see Pins

and Bonnet 1996; Stafford and Gurney 2004; van Maanen et al. 2012; Reina et al. 2018).

After having established that the two models under consideration (LCA and mDDM) both show magnitude-sensitivity for the parameter sets employed here, in the next section, we present our detailed results on the sensitivity to the frequency of input signals (in conjunction with magnitude-sensitivity) the LCA and mDDM exhibit.

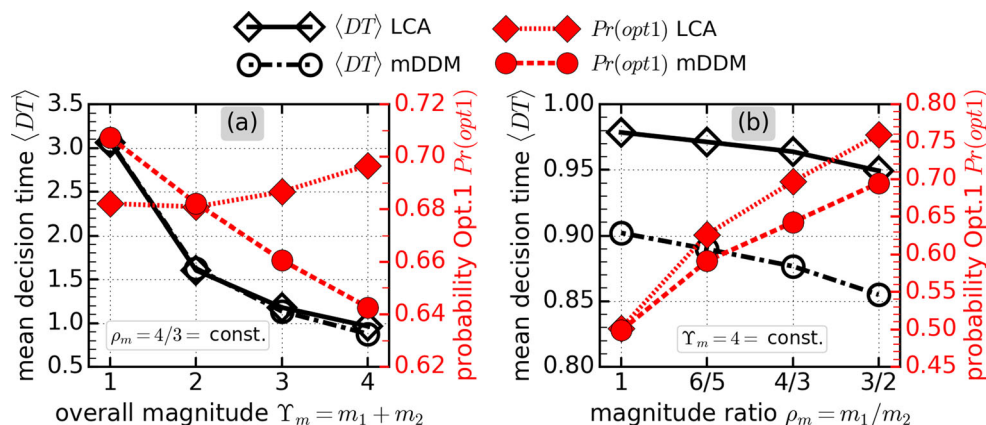
Performance Under Periodic Signal Stimuli

Mean Decision Time and Choice Probability for Pulsed Stimulus Condition SC1

Periodic signals were applied under the two stimuli conditions SC1 and SC2, which are summarised in Table 1. In Fig. 4a, we show mean decision times $\langle DT \rangle$ and probabilities of choosing option 1, $\text{Pr}(\text{opt1})$, depending on both varying magnitude ratios and varying frequency ratios for SC1 when Υ_f and Υ_m are kept constant. In condition SC1, both stimuli are in high-magnitude mode for 50% of the time and the stimulus frequency determines the pulse width and the width between two high-magnitude pulses (see Fig. 1a).

The performance of the LCA model is illustrated in the left column in Fig. 4a. If the frequency ratio is fixed whilst the magnitude ratio varies, we see that $\langle DT \rangle$ has maxima around $\rho_m \approx 1$ (Fig. 4a, top-left). For larger as well as smaller ρ_m , the mean decision time decreases. The reason for this behaviour is that evidence accumulation takes longer if the stimuli are equal, or almost equal, compared with the case when stimuli may be easily discriminated. This is further underlined by the plot of $\text{Pr}(\text{opt1})$ for the LCA in the bottom-left panel in Fig. 4a. For magnitude ratios $\rho_m \approx 1$, we find that $\text{Pr}(\text{opt1}) \approx 0.5$, i.e. option 1 and option 2 are both chosen in 50% of all trials. However, if instead we look at the effect of changing frequency ratios when the magnitude ratio is fixed, we observe that $\langle DT \rangle$ (Fig. 4a, top-left) and $\text{Pr}(\text{opt1})$ (Fig. 4a, bottom-left)

Fig. 3 Mean decision time and probability of choosing option 1 depending on the overall magnitude (a) and depending on the magnitude ratio (b). Results shown relate to the distributions in Fig. 2. LCA model (5) and mDDM (Eqs. 3 and 4) are compared, based on the simulation of 10^5 trials for each model and condition



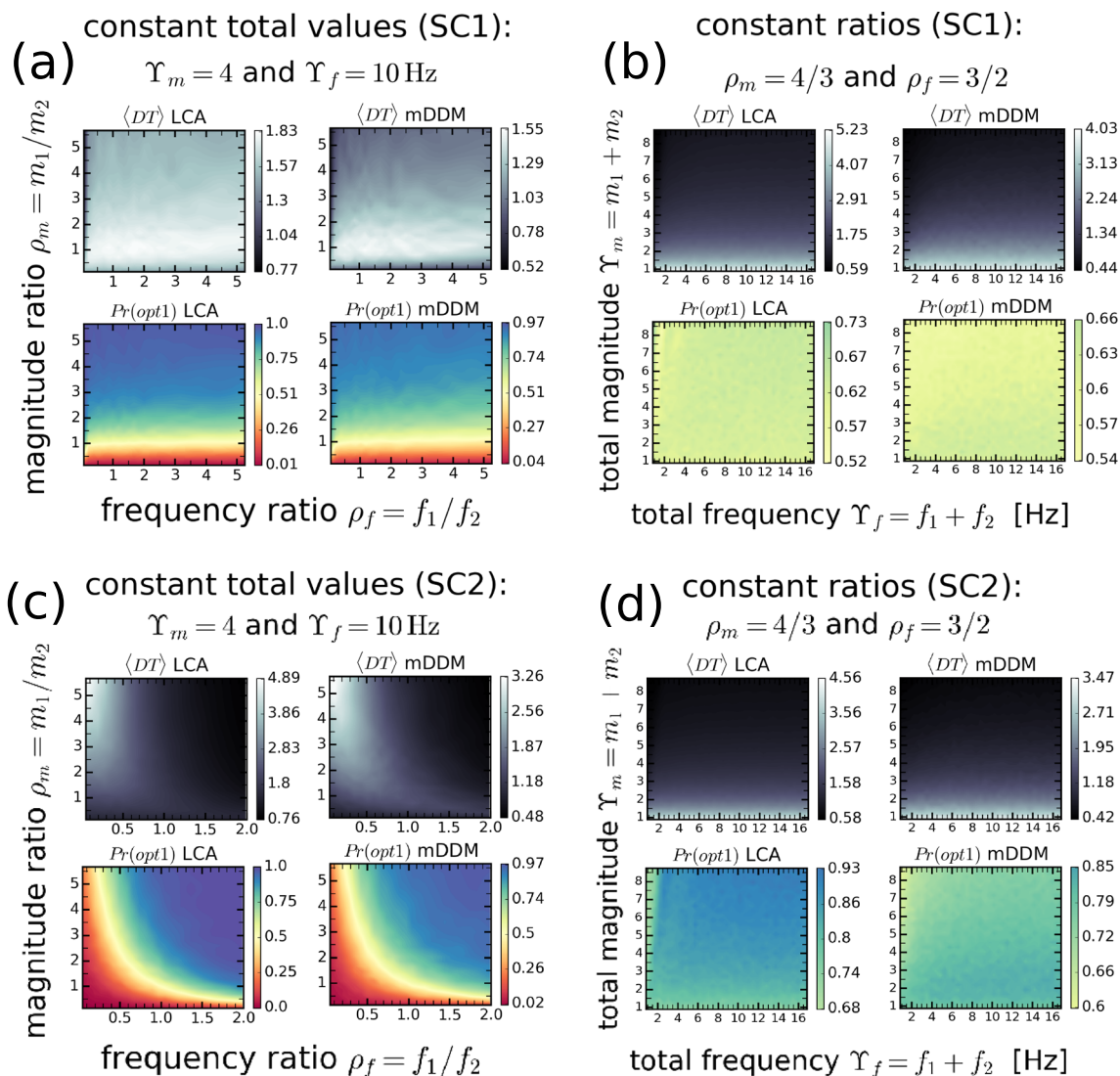


Fig. 4 Mean decision time and probability of choosing option 1 depending on magnitude ratios, frequency ratios, total magnitudes and total frequencies under stimulus conditions SC1 and SC2 (see Table 1). LCA model (5) and mDDM (Eqs. 3 and 4) are compared, based on the

show less variation. Nevertheless, we find a significant frequency ratio-dependent effect which is more clearly demonstrated in Figs. 5a and 6a. Here, we plotted $\langle DT \rangle$ and $Pr(opt1)$ for selected magnitude ratios and a smaller range of frequency ratios. The behaviour of both quantities is symmetric around $\rho_f = 1$ because of the fixed overall frequency Υ_f . This means that $\langle DT \rangle$ in Fig. 5a increases (decreases) monotonously if $\rho_f < 1$ ($\rho_f > 1$), whereas $Pr(opt1)$ in Fig. 6a shows the inverse behaviour. Additionally, we note that the two curves labelled $\rho_m = 1/3$ and $\rho_m = 3$ in Figs. 5a and 6a, respectively, represent equivalent cases (but with opposing response probabilities) for constant Υ_m and Υ_f . Furthermore, the simultaneous occurrence of an increase of $\langle DT \rangle$ and a decrease of $Pr(opt1)$ indicate that a decrease of performance when alternatives

simulation of 2000 trials for each model and data point. Colour bars for $Pr(opt1)$ are normalised such that $0 \leq Pr(opt1) \leq 1$ for both models and all conditions. Decision time plots are not normalised to improve qualitative comparison between both models. $\langle DT \rangle$ is given in seconds

are presented more often but with shorter pulse widths (i.e. less continuous) while maintaining identical duty cycles.

If we look at the corresponding results for the mDDM in the right column in Fig. 4a, and Figs. 5d and 6d, we see that the mDDM behaves similarly compared with the results regarding the behaviour of the LCA model. Because of this qualitative agreement, the same analysis applies to the mDDM results.

To study the effect of varying overall frequencies and magnitudes, Υ_f and Υ_m , under condition SC1 when magnitude and frequency ratios remain constant, we refer to Fig. 4b. Again, the results shown for LCA (Fig. 4b, left column) and those relating to the mDDM (Fig. 4b, right column) are qualitatively very similar. For fixed overall frequencies in the range shown, an increase of Υ_m leads to

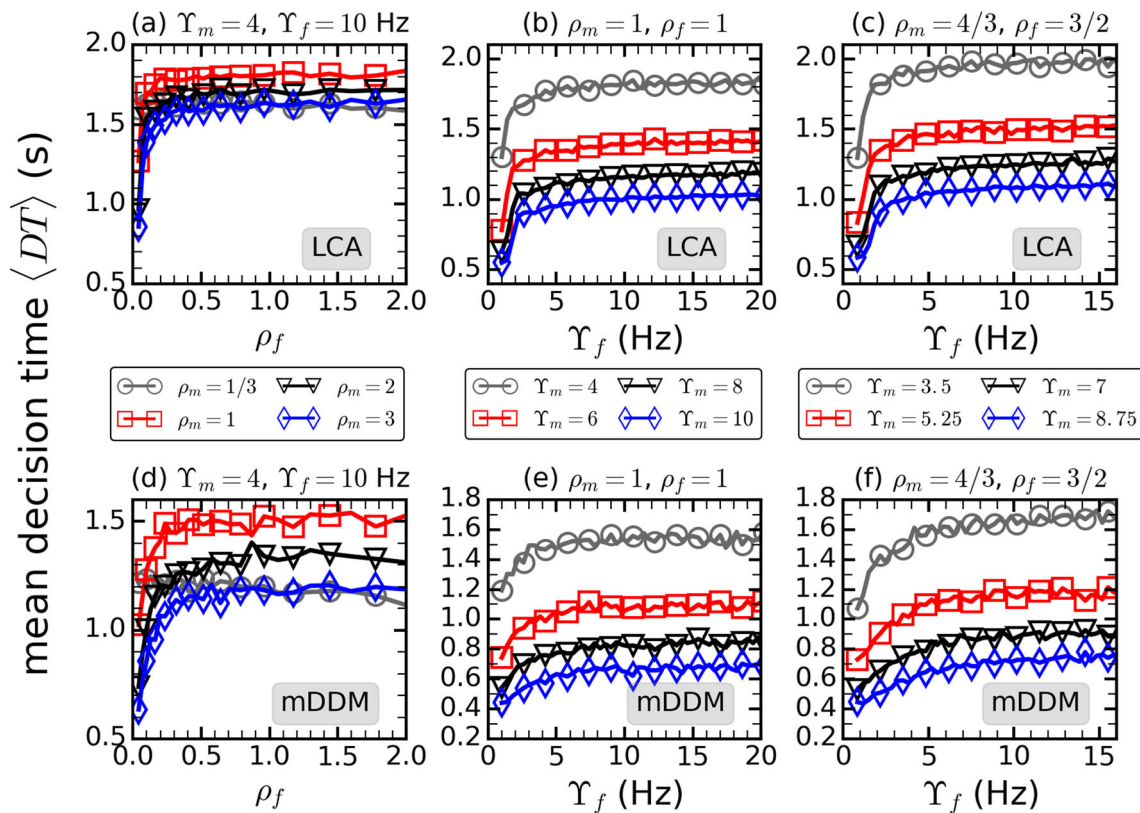


Fig. 5 Mean decision time depending on frequency ratio and overall frequency under stimulus condition SC1 (see Table 1). The behaviour for different values of overall magnitudes and magnitude ratios is compared. **a, d:** Υ_m and Υ_f are fixed; **b–c** and **e–f:** ρ_m and ρ_f are

fixed. LCA model (**a–c**, Eq. 5) and mDDM (**d–f**, Eqs. 3 and 4) are compared, based on the simulation of 2000 trials for each model and data point

a decrease of $\langle DT \rangle$ which is an effect of the multiplicative noise. Although less pronounced compared with the effect of changing Υ_m , a variation of Υ_f when fixing the overall magnitude shows a frequency-sensitive effect, which is emphasised for LCA and mDDM in Fig. 5c, f. For both models, we see that an increase of the overall frequency Υ_f causes an increase of the mean decision time. This effect is stronger for smaller Υ_f and becomes less pronounced for larger Υ_f . Quantitatively, we observe that the change of the slope characterising the increase of $\langle DT \rangle$ with increasing Υ_f occurs at $\Upsilon_f \approx 2$ Hz (LCA, Fig. 5c) and $\Upsilon_f \approx 5$ Hz (mDDM, Fig. 5f), respectively. We assume, however, that these values most likely depend on the parameter set chosen. The increase of $\langle DT \rangle$ further underpins our hypothesis that having options presented more discontinuously (i.e. more pulses with shorter pulse widths) whilst duty cycles are maintained increases decision times, and therefore lowers the decision-making performance.

In addition, $\text{Pr}(\text{opt1})$ shows only little variation for varying Υ_f and fixed Υ_m , as can be seen in Fig. 4b for the whole range of absolute magnitudes used in our study, and in Fig. 6c, f for selected Υ_m . Here, $\text{Pr}(\text{opt1})$ seems to remain almost constant under the variation of Υ_f except for some

fluctuations due to the presence of noise. However, we can also see that $\text{Pr}(\text{opt1}) \geq 0.52$ for LCA (Fig. 4b, bottom-left) and $\text{Pr}(\text{opt1}) \geq 0.54$ for mDDM (Fig. 4b, bottom-right) for all values of the overall magnitude and the overall frequency, which results from option 1 being the higher-magnitude option ($\rho_m = 4/3 > 1$). We also point out that the magnitude-sensitive results for periodic stimuli are in agreement with the magnitude-sensitive results obtained for constant stimuli discussed in the “Performance Under Stimuli with Constant Magnitude” section (see Fig. 3 for comparison). Considering equal alternatives ($\rho_m = 1, \rho_f = 1$), we can see that results are similar to the unequal alternatives case, as shown in Figs. 5b, e and 6b, e. However, as expected, we find that $\text{Pr}(\text{opt1})$ varies only slightly around 0.5 (Fig. 6b, e).

A comparison of LCA and mDDM for different simulated frequency and magnitude conditions under SC1 is also presented in the quantile-probability plots in Fig. 7a, c. Again, we see that qualitatively LCA and mDDM show similar behaviour. In particular, for both models, there seems to be little variation of the decision times with response proportions under SC1. A similar behaviour in quantile-probability plots has been observed by Ratcliff et al. (2018).

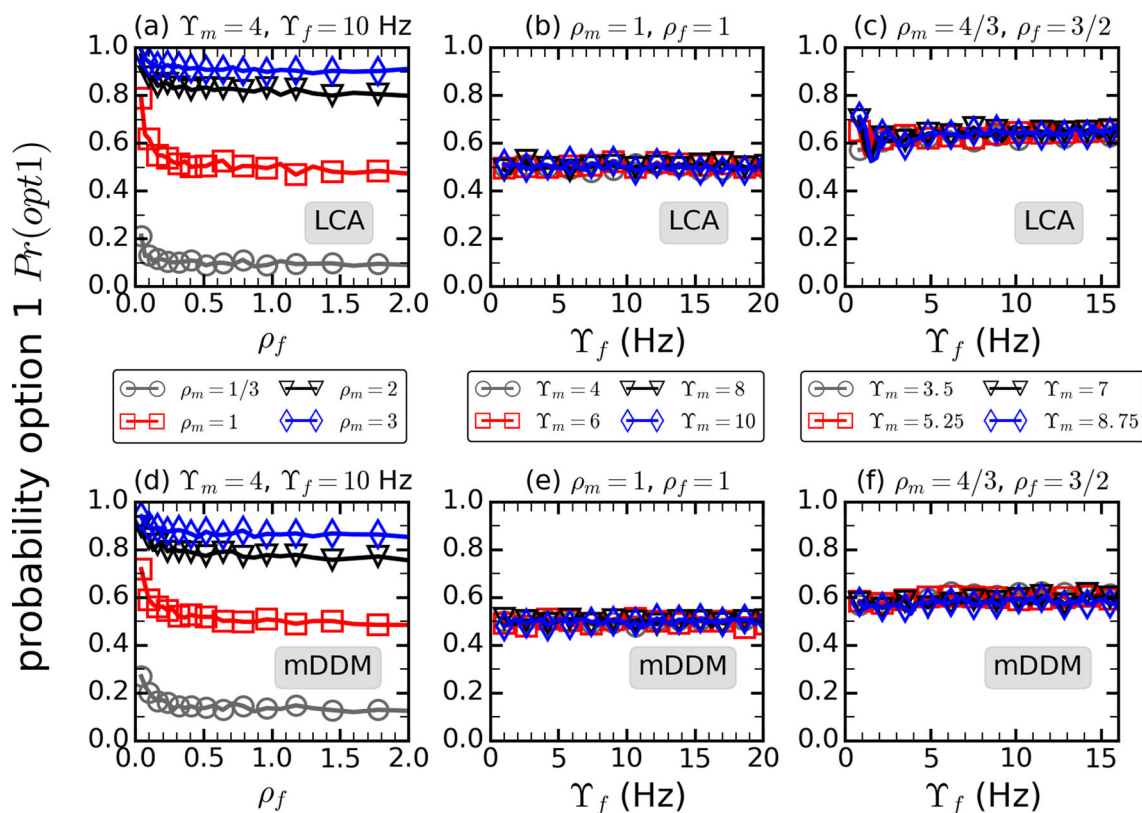


Fig. 6 Probability of choosing option 1 depending on frequency ratio and overall frequency under stimulus condition SC1 (see Table 1). The behaviour for different values of overall magnitudes and magnitude ratios is compared. **a, d:** Υ_m and Υ_f are fixed; **b–c** and **e–f:** ρ_m and ρ_f

are fixed. LCA model (**a–c**, Eq. 5) and mDDM (**d–f**, Eqs. 3 and 4) are compared, based on the simulation of 2000 trials for each model and data point

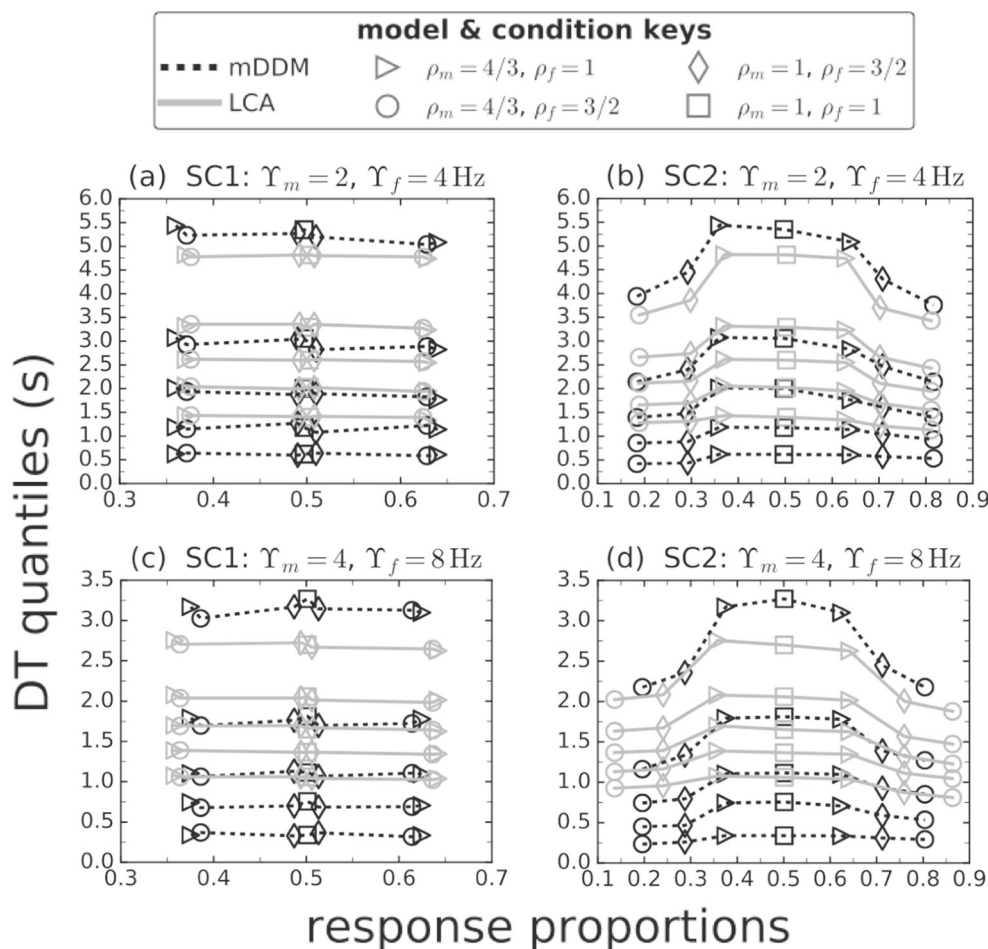
Mean Decision Time and Choice Probability for Pulsed Stimulus Condition SC2

The behaviour of $\langle DT \rangle$ and $\text{Pr}(\text{opt}1)$ relating to stimulus condition SC2 is shown in Fig. 4c, d. Recall that under this condition, the duty cycle of signal 1 is proportional to the frequency ratio $\rho_f = f_1/f_2$, whereas the duty cycle of signal 2 is held constant at 0.5 (see Table 1). In Fig. 4c, where overall magnitudes and frequencies remain unaltered, we see once more that the LCA model and mDDM behave similarly. Therefore, we discuss them simultaneously. The simulation of both models demonstrates that there is a nonlinear relationship between magnitude ratios and frequency ratios along which $\text{Pr}(\text{opt}1) \approx 0.5$, i.e. both alternatives are chosen equally often (Fig. 4c, bottom-left and bottom-right). In terms of evidence accumulation, this in turn indicates that there may be an equivalence between varying frequencies and magnitudes of two options such that it is hard to discriminate between them when they are presented under stimulus condition SC2. In addition, by inspecting the $\langle DT \rangle$ -plots together with the $\text{Pr}(\text{opt}1)$ -plots (left column in Fig. 4c for LCA and right column in Fig. 4c for mDDM), we can see that close to the area

where $\text{Pr}(\text{opt}1) \approx 0.5$ the mean decision time increases, as it becomes harder to distinguish both stimuli.

To better illustrate the behaviour of $\langle DT \rangle$ and $\text{Pr}(\text{opt}1)$ for varying frequency ratios, we depict both quantities for selected ρ_m in Figs. 8a, c, and 9a, c, respectively. Comparing the curves characterised by different ρ_m , we observe that an increase of ρ_m leads to an increase of $\langle DT \rangle$ for $\rho_f < 1$, and to a decrease of $\langle DT \rangle$ for $\rho_f > 1$, i.e. the order of the curves for different ρ_m is inverted at $\rho_f \approx 1$. Under SC2, $\rho_f = 1$ is the frequency ratio where the duty cycles of both input signals are equal. All other frequency ratios lead to unequal duty cycles, which explain the observed behaviour. A larger ρ_f , and hence a larger duty cycle, is tantamount to increased evidence, as is a larger magnitude ratio. Therefore, the distinct behaviour observed below and above $\rho_f \approx 1$ results from the joint effect of varying frequency and magnitude ratios on the evidence integrated. Inspecting the shape of $\langle DT \rangle$ depending on ρ_f , we see that the mean decision time has a maximum which is shifted towards smaller ρ_f when ρ_m is increased. This effect applies to both models, LCA (see Fig. 8a) and mDDM (see Fig. 8c), although the mDDM displays the maximum more clearly, which is probably due to the specific parameter sets chosen for each model.

Fig. 7 Plot of decision time quantiles versus response proportions for varying frequency and magnitude conditions, and different stimulus conditions (SC1 and SC2). LCA and mDDM (encoded by grayscale and linestyle) are compared based on four different conditions (encoded by symbol) as indicated in the model/conditions key (see top of plot). For each condition, response proportions are plotted along the horizontal axis and decision time quantiles (0.1, 0.3, 0.5, 0.7, 0.9) for both responses in favour of option 1 and option 2 are plotted vertically. Choices in favour of option 1 are shown with response proportions greater than 0.5. Both models (LCA and mDDM) show similar qualitative behaviour in each stimulus condition. Varying the stimulus condition changes the shape of the decision time quantiles plotted along response proportions. An increase of the overall magnitude leads to a decrease of decision time



Furthermore, increasing either ρ_f or ρ_m , or both, increases $\text{Pr}(\text{opt1})$ (see Figs. 4c and 9a, c), as increasing either of the two ratios increases evidence for option 1 under SC2.

Mean decision time plots and corresponding choice probabilities depending on Υ_f are illustrated for constant $\rho_m = 4/3$ and constant $\rho_f = 3/2$ in Figs. 4d, 8b, d and 9b, d. Comparing the behaviour of $\langle \text{DT} \rangle$ in Figs. 4d and 8b, d with the equivalent plots obtained under condition SC1 (Figs. 4b and 5c, f), it becomes obvious that both models, LCA and mDDM, show the same qualitative behaviour under SC1 and SC2, that is $\langle \text{DT} \rangle$ increases with increasing Υ_f . Quantitatively, however, we find smaller values for $\langle \text{DT} \rangle$ if the pulsed stimuli are presented under SC2. This effect can be attributed to the direct proportionality between DC1 and ρ_f in SC2. This proportionality is not present in SC1. If we compare the behaviour of $\text{Pr}(\text{opt1})$ obtained under SC2 (Figs. 4d and 9b, d) with the results for condition SC1 (Fig. 4b and 6c, f), it becomes obvious that under SC2, $\text{Pr}(\text{opt1})$ increases for smaller Υ_f and seems to saturate for larger Υ_f . This increase of $\text{Pr}(\text{opt1})$ for small Υ_f is not present when the models are simulated under SC1. We also note that assuming $\rho_f = 1 = \rho_m$ makes conditions SC1 and SC2 equivalent. Therefore, all results

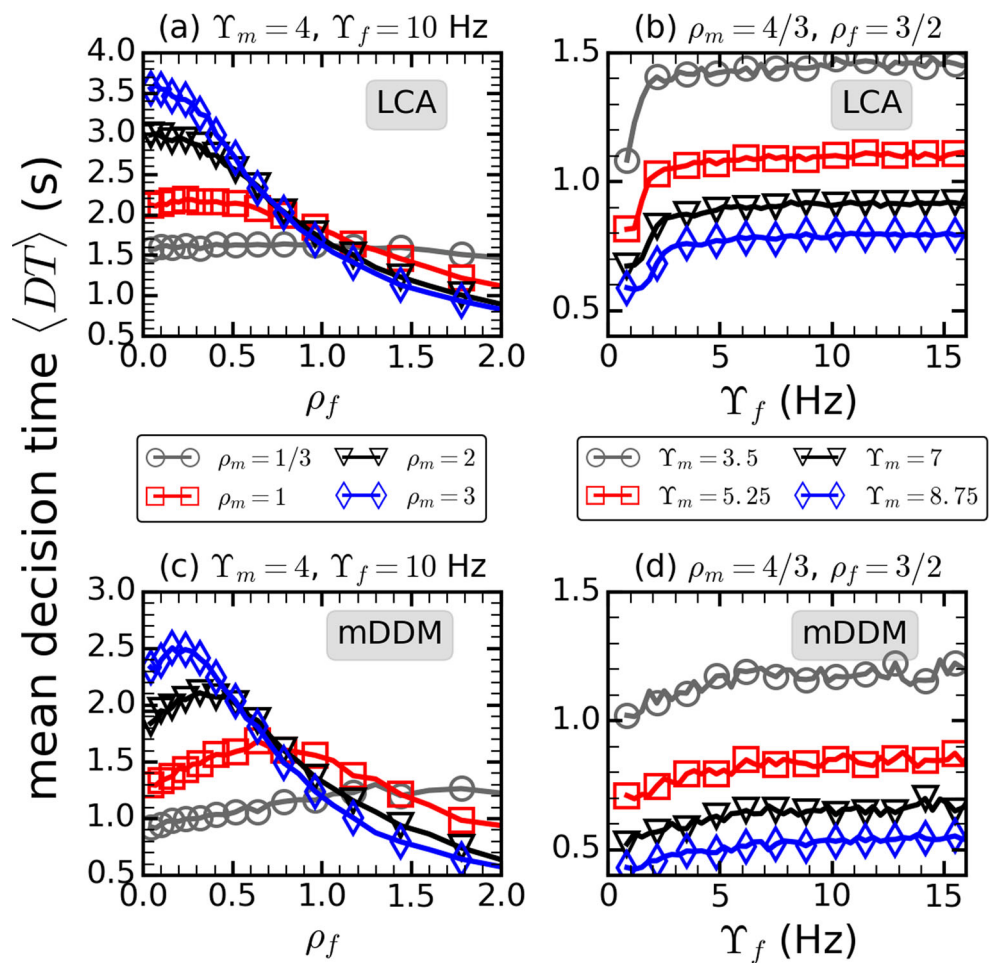
discussed for Figs. 5b, e and 6b, e also apply to stimulus condition SC2.

An overview of how decision time quantiles computed under SC2 compare with those simulated under SC1 for various conditions can be obtained by a comparison of Fig. 7a, c with b, d. Response proportions corresponding to different conditions become more separated along the horizontal axis under SC2 and whereas the decision time quantiles remained almost constant across conditions under SC1 (Fig. 7a, c), we can notice increasing decision times if response proportions move towards 0.5 under SC2 (Fig. 7b, d).

Decision Time Distributions Under Periodic Stimuli

Decision time distributions which relate to condition SC1 are shown in Fig. 10 for varying ρ_f , ρ_m , Υ_f and Υ_m . To create the distribution plots, we divided the simulated data into bins and then connected the bin centres with an interpolated function. Strikingly, we observe that the frequency of the stimuli clearly shapes the decision time distribution functions obtained from both LCA model and mDDM. In Fig. 10a, c, i, k, we have $f_1 = f_2$ ($\rho_f = 1$) and

Fig. 8 Mean decision time depending on frequency ratio and overall frequency under stimulus condition SC2 (see Table 1). The behaviour for different values of overall magnitudes and magnitude ratios is compared. **a, c:** Υ_m and Υ_f are fixed; **b, d:** ρ_m and ρ_f are fixed. LCA model (**a, b;** Eq. 5) and mDDM (**c, d;** Eqs. 3 and 4) are compared, based on the simulation of 2000 trials for each model and data point



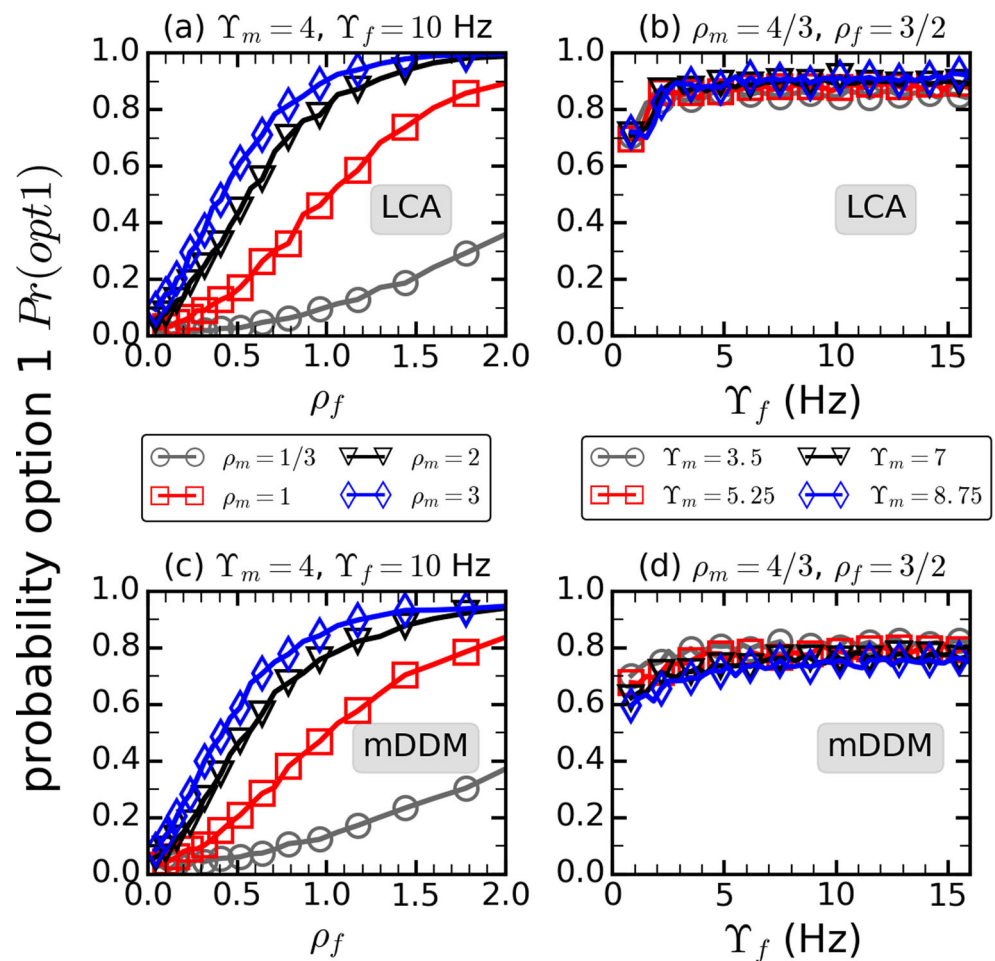
$m_1 = m_2$ ($\rho_m = 1$). In these plots, it can most clearly be seen that the signal frequency is reproduced in the response times. Specifically, the frequencies used are $f_1 = f_2 = 2$ Hz (Fig. 10a, i) and $f_1 = f_2 = 4$ Hz (Fig. 10c, k). The corresponding decision time distributions show exactly 2 peaks (Fig. 10a, i) or 4 peaks (Fig. 10c, k), respectively, per second.

In case of $\rho_f = 3/2$, we see another direct effect on the modulation of the distribution function. For example, the simulation of the mDDM in Fig. 10l yields an additional frequency pattern, which recurs every 0.625 s. This is exactly equal to $1/|f_1 - f_2| = 1/1.6$ s, i.e. given by the difference of the frequency between both stimuli. Similarly, we can also identify the signal frequency 9.6 Hz in the decision time distribution plots for mDDM and LCA in Fig. 10l, which is equal to $2 f_1$. These effects are most likely due to the nonlinearity of the decision time distribution as a function of the periodic inputs, $I_1(t)$ and $I_2(t)$, which may lead to a modulation of the original inputs such that the modified inputs may also contain sum and difference of the original frequency. In case of the mDDM, the multiplicative noise term in Eq. 4 may also contribute to the modulation

of the original inputs. Furthermore, increasing the overall magnitude leads to an effect equivalent to our observation in the constant, nonperiodic stimuli (cf. Fig. 2a–d). Higher Υ_m make the shape of the decision time distribution narrower and shift it to lower decision times.

Equivalent decision time distributions that relate to condition SC2 are shown in Fig. 11. Generally, we can make similar observations compared with stimulus condition SC1 depicted in Fig. 10. Employing SC2, the periodic pattern in the distribution also derives from the periodicity in the pulsed stimuli for all combinations of ρ_f , ρ_m , Υ_f and Υ_m plotted in Fig. 11. In particular, all plots with $\rho_f = 1$ in Fig. 11 are identical to those with $\rho_f = 1$ in Fig. 10. This was expected, as stimulus conditions SC1 and SC2 coincide for frequency ratios $\rho_f = 1$. However, as the duty cycle of signal 1 increases with ρ_f in SC2, we can also see that for $\rho_f = 3/2$ decision time distributions derived under SC2 in Fig. 11 are a bit narrower and shifted towards lower decision times compared with the equivalent distributions obtained for $\rho_f = 3/2$ under condition SC1 in Fig. 10. This results from the duty cycle of signal 1 being proportional to $\rho_f = f_1/f_2$ in condition SC2.

Fig. 9 Probability of choosing option 1 depending on frequency ratio and overall frequency under stimulus condition SC2 (see Table 1). The behaviour for different values of overall magnitudes and magnitude ratios is compared. **a, c:** Υ_m and Υ_f are fixed; **b, d:** ρ_m and ρ_f are fixed. LCA model (**a, b;** Eq. 5) and mDDM (**c, d;** Eqs. 3 and 4) are compared, based on the simulation of 2000 trials for each model and data point



Requirements to Observe Periodicities in Decision Time Distributions Due to Periodic Stimuli

Analysis of Decision Time Distributions

An important requirement to observe periodicity in decision time distributions concerns the choice of the bin width, which should be small enough to detect the periodic pattern. This is equivalent to the reconstruction of periodic signals known from signal processing theory: the highest frequency (Nyquist frequency) that can be detected in a periodic signal is half the sampling rate. In our terms, we therefore require sufficiently small bin-widths w_b , such that $1/w_b \geq 2 f_{\text{signal}}$, to find the decision time distributions corresponding to the periodic stimuli occurring with f_{signal} . This is demonstrated in Fig. 12. If bin-widths are too large, we detect the wrong frequency (Fig. 12a). When choosing $1/w_b = f_{\text{signal}}$ exactly, then no frequency can be detected at all, as shown in Fig. 12b. This is a strong indication that the frequency of the periodic stimulus directly translates into the periodicity of the decision time distribution. We depict in Fig. 12c that only if the bin-width is chosen sufficiently small, the correct distribution may be reconstructed.

Possibility of Loss of Periodic Information of External Stimulus

Our theoretical study makes the prediction that periodic decision time distributions could possibly be observed in real decision-makers. However, it may also be possible that stimulus oscillations are smoothed when they are transduced into evidence that is accumulated. It might as well be the case that the periodic oscillations of the stimuli are partly smoothed and partly transduced. The latter is the more general scenario and to include it in the models used in this paper we can replace \tilde{S} in Eq. 2 with

$$\tilde{S}_j(t) = \kappa S_j(t) + (1 - \kappa) \langle S_j(t) \rangle + \epsilon(t), \tag{6}$$

where κ is a smoothing factor, $\epsilon(t)$ is a normally distributed variable sampled from $\mathcal{N}(\text{mean} = 0, \text{SD} = 0.05)$ at each timestep, $S(t)$ is the stimulus signal introduced in Eq. 1 and $\langle S_j(t) \rangle = 1/T_j \int_0^{T_j} S_j(t) dt$, where T_j denotes the period of stimulus signal j , is the averaged input, which can be expressed as

$$\langle S_j(t) \rangle = m_j DC_j + 0.2(1 - DC_j), \tag{7}$$

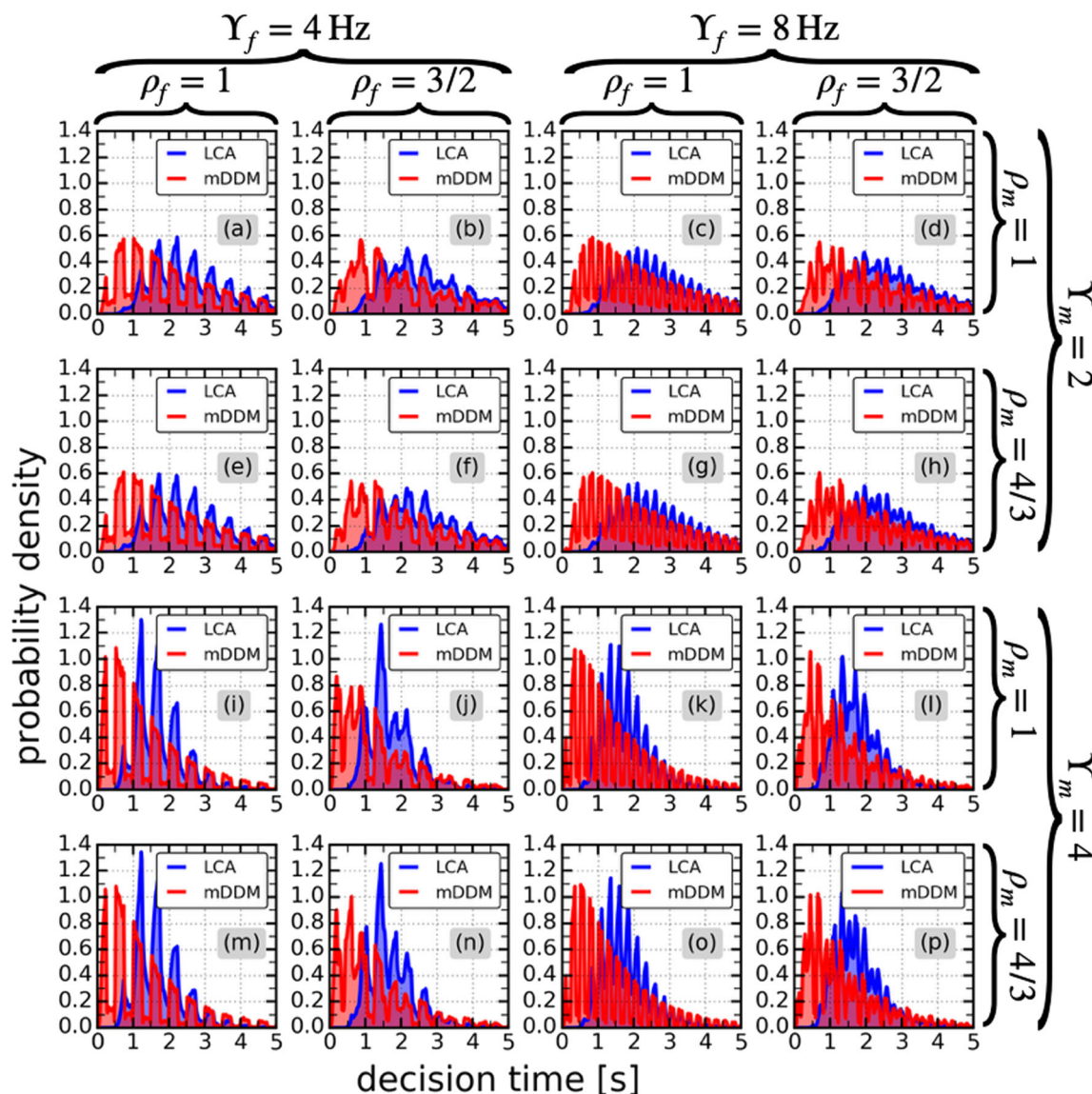


Fig. 10 Decision time distribution (probability density) for periodic stimulus condition SC1 (see Table 1), depending on ρ_m , ρ_f , Υ_m and Υ_f (see Table 2). LCA model (5) and mDDM (Eqs. 3 and 4) are compared, based on the simulation of 10^5 trials for each model and condition. Distributions shown are normalised histograms, where

where, as before, DC_j is the duty cycle of stimulus j and m_j is its magnitude.

The introduction of the smoothing factor κ allows describing the transition between complete transduction of the external stimulus oscillations into the internal input signal ($\kappa = 1$) and smoothing of the input signal oscillations ($\kappa = 0$), in which case the periodicity of the external stimulus would be lost. For $0 < \kappa < 1$, we have a superposition of the effects of smoothing and transducing the oscillations of the external stimulus into its internal representation. The effect of varying κ on the shape of the decision time distribution is shown in Fig. 13. We can see that for $\kappa = 0$ (Fig. 13a), the signal is smoothed and that there is no

the coloured area under the curve equals 1. The bin-width is narrow ($0.025 \cong 200$ bins for the decision time interval shown). The curve superposing the histogram goes through the centers of the bins and is interpolated in between

periodicity observable in the decision time distribution. Increasing κ introduces periodic patterns in the decision time distribution (Fig. 13b–h). Furthermore, it seems to be the case that, at least for the parameter configuration studied here, rather small values of κ (e.g. see Fig. 13c, d) are sufficient to induce periodic patterns in the decision time distribution. How this may generalise to other parameter configurations, however, needs further investigation.

Proposal of an Experimental Design

As our study was motivated by brightness discrimination tasks previously investigated by Teodorescu et al. (2016),

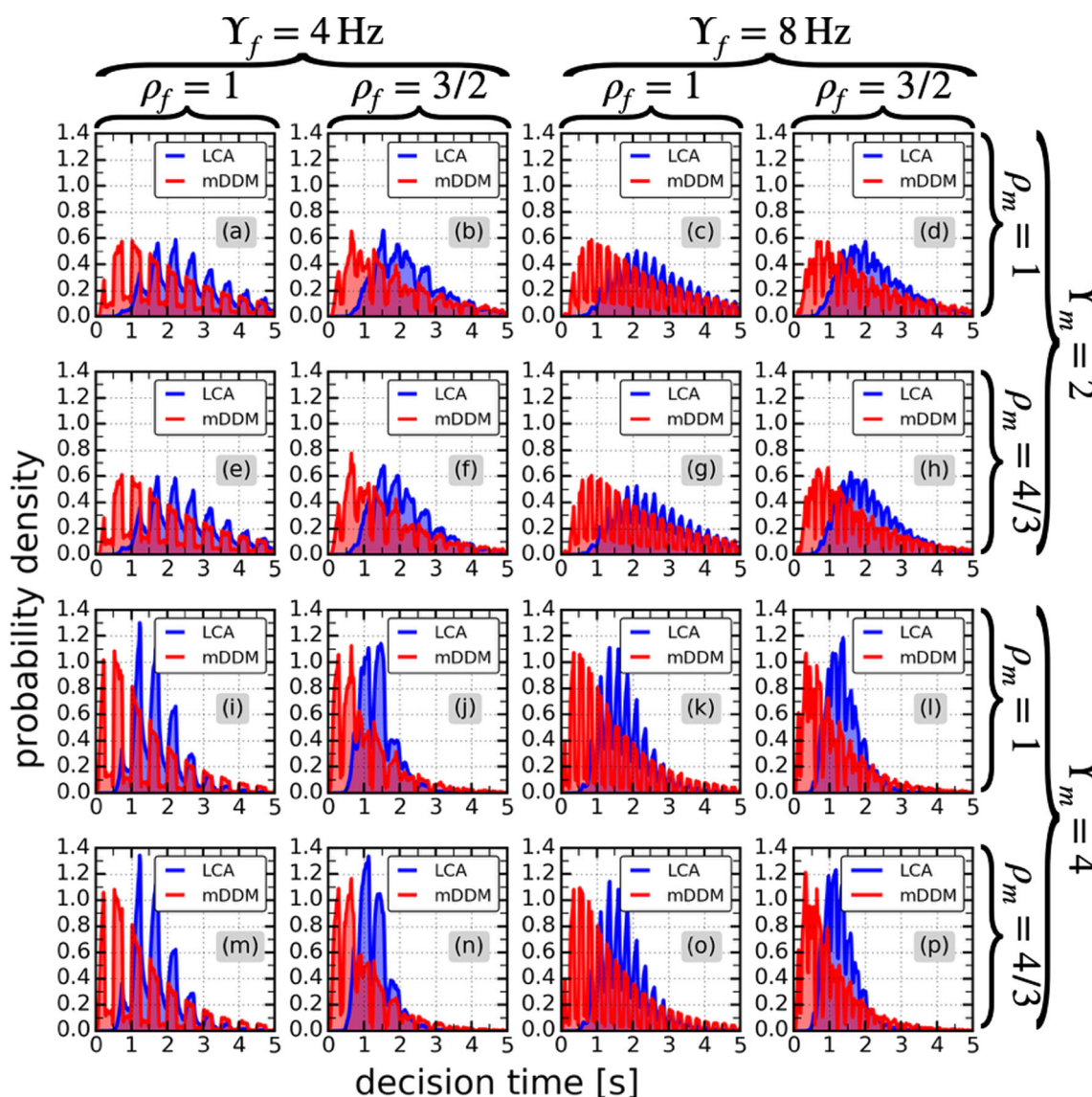


Fig. 11 Decision time distribution (probability density) for periodic stimulus condition SC2 (see Table 1), depending on ρ_m , ρ_f , Υ_m and Υ_f (see Table 2). LCA model (5) and mDDM (Eqs. 3 and 4) are compared, based on the simulation of 10^5 trials for each model and condition. Distributions shown are normalised histograms, where

the coloured area under the curve equals 1. The bin-width is narrow ($0.025 \cong 200$ bins for the decision time interval shown). The curve superposing the histogram goes through the centers of the bins and is interpolated in between

Pirrone et al. (2018) and Ratcliff et al. (2018), we believe that a similar experimental approach would be suitable to test our predictions. In particular, we emphasise that the presence of a strong coupling between external stimulus and its internal representation (cf. Eq. 2) is a crucial assumption in our modelling study and that empirical support for this assumption was provided by Teodorescu et al. (2016) and Ratcliff et al. (2018). For a detailed description of previous implementations of this brightness discrimination task, we refer to the articles by Teodorescu et al. (2016) and Ratcliff et al. (2018); see also Pirrone et al. (2018) who implemented a task similar to the one studied by Teodorescu et al. (2016).

In what follows, we adopt and summarise the key features of the aforementioned brightness discrimination task, including our assumption to present external stimuli periodically with a well-defined frequency. The task comprises the presentation of two homogeneous grey patches on a black background (round patches with a diameter of 1.2 cm and centre-to-centre distance of 6.2 cm in Teodorescu et al. (2016) and Pirrone et al. (2018), and square patches presented at a standard viewing distance of 53 cm, each patch being 3.24 degrees tall by 3.24 degrees wide with the two arrays covering 8.64 degrees from edge to edge in Ratcliff et al. (2018)). On each trial, the grey patches were

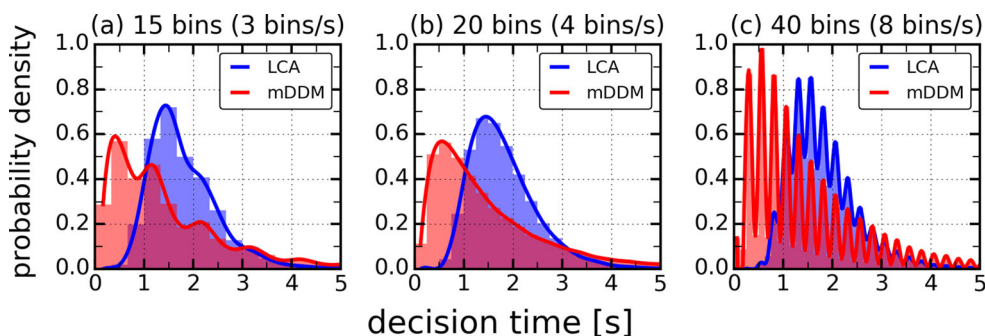


Fig. 12 Decision time distribution (probability density) depending on the bin-width (or number of bins, respectively) for magnitude ratio $\rho_m = 1$ and frequency ratio $\rho_f = 1$, i.e. this figure applies to both stimulus conditions SC1 and SC2 (see Table 1). The same distribution is shown in Fig. 10k in Fig. 11k for distributing the data over 200 bins (i.e. 40bins/s). The magnitudes are $m_1 = m_2 = 2$ and the frequencies

take values $f_1 = f_2 = 4$ Hz. LCA model (5) and mDDM (Eqs. 3 and 4) are compared, based on the simulation of 10^5 trials for each model. Distributions shown are normalised histograms, where the coloured area under the curve equals 1. The curve superposing the histogram goes through the centers of the bins and is interpolated in between

fluctuating over time and individual patch grey-levels were re-sampled from a normal distribution on each monitor frame at a refresh rate of 60 Hz. The magnitude mean values of the corresponding distributions varied across trials but were constant within a trial. Whereas Teodorescu et al. (2016) and Ratcliff et al. (2018) studied various conditions where the mean values of the normal distributions used for brightness magnitude sampling were different for each stimulus, Pirrone et al. (2018) also looked at several equal alternative cases with equal mean values of the underlying

distributions. In our theoretical study, we observed frequency effects in the decision time distribution in both cases when external stimuli were presented periodically. Hence, we think that both equal and unequal alternatives could potentially be used to detect periodic patterns in the decision time distribution in empirical studies using periodically pulsed stimuli. For an experimental implementation, the choice of the brightness levels could be adopted from previous studies (Teodorescu et al. 2016; Pirrone et al. 2018; Ratcliff et al. 2018).

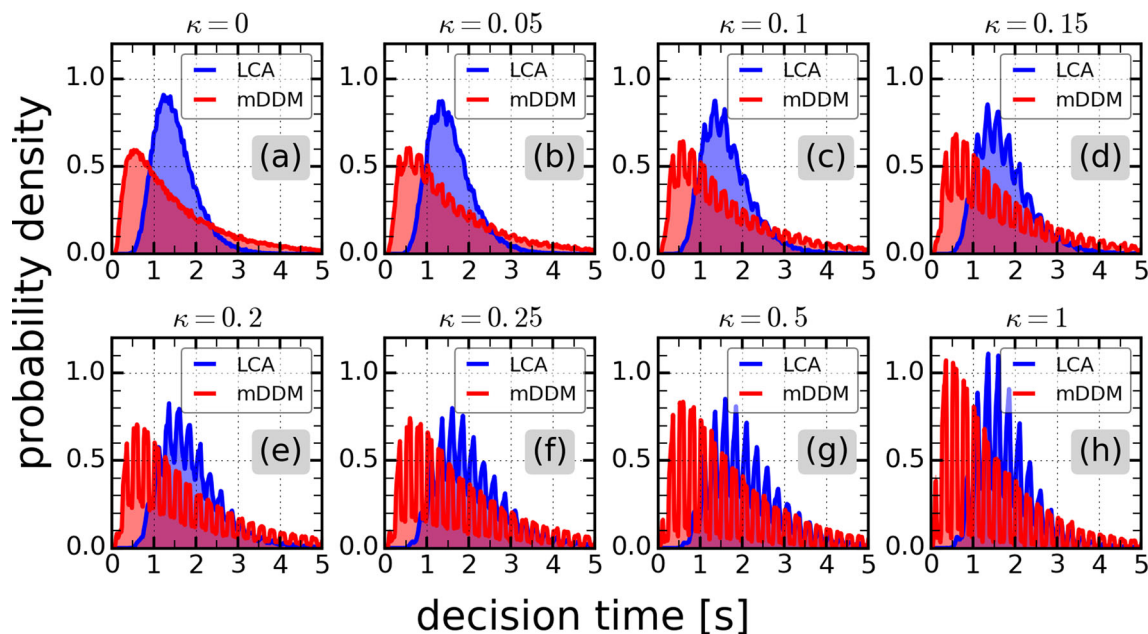


Fig. 13 Effect of smoothing factor κ on the periodicity of decision time distributions. A value of $\kappa = 0$ means that all periodicity is lost, values in the range $0 < \kappa < 1$ corresponds to a superposition of transducing oscillations of the external input signal and smoothing, and $\kappa = 1$ represents the case when the periodicity of the external stimulus is fully transduced into its internal representation. A small nonzero value of κ should be sufficient to yield periodic patterns in the decision

time distribution following the presentation of periodic stimuli as discussed in the text. The chosen overall magnitudes and frequencies and their respective ratios are: $\Upsilon_m = 4$, $\Upsilon_f = 8$, $\rho_m = 1 = \rho_f$. Distributions shown are normalised histograms, where the coloured area under the curve equals 1. The bin-width is narrow ($0.025 \cong 200$ bins for the decision time interval shown). The curve superposing the histogram goes through the centers of the bins and is interpolated in between

Regarding the choice of the frequency, we propose to use a suitable window for which it could be possible to observe periodicities in decision time distribution due to the periodic presentation of external stimuli. That is, the stimulus frequency should neither be chosen too large, as evidence integration may not be able to recognise the frequency pattern, nor too small, as threshold conditions may be met already before the brightness magnitude could fluctuate for a sufficient number of times to be transduced into the internal decision variable. Therefore, we propose that a suitable frequency interval to test our prediction should be in the range of 0.5 – 10 Hz, which we also used in the present paper. This frequency window corresponds to timescales in the range of 100 ms – 2 s, which covers the typical range for sensory processing involved in cognitive tasks (~ 100 ms) (Mauk and Buonomano 2004; Kiebel et al. 2008) but also typical decision times ~ 1 s obtained under laboratory conditions (e.g. see Ratcliff et al. 2016, and references therein). In addition, this frequency range is well separated from stimulus refresh rate of 60 Hz, which was used in empirical studies (Teodorescu et al. 2016; Pirrone et al. 2018; Ratcliff et al. 2018). This separation will allow to clearly discriminate frequency effects discussed in this paper from those that may arise from stimulus re-sampling. For example, stimulus presentation in the time domain could follow the temporal profiles shown in Fig. 1, i.e. employing external stimuli with clearly recognisable deterministic oscillations and random fluctuations added that have higher frequency and significantly smaller magnitudes.

Based on our results discussed in the previous section, an experimental realisation should also aim at yielding a smoothing factor of $\kappa > 0$ in order to observe periodic patterns in decision time distributions that result from external periodic stimuli. A variation of the duty cycle might help to achieve this. In other areas of neuroscience such as the optogenetic investigation of neural circuits, for example, the duty cycle of a stimulus has been identified as a relevant parameter which may be varied to optimise stimulation (Tye and Deisseroth 2012).

Discussion

Effects of Varying Magnitude and Frequency Conditions

Assuming a strong coupling between external stimulus input and internal stimulus representation (see Eq. 2), we have simulated and compared two decision-making models, LCA and mDDM, under periodically oscillating stimuli. Variants of both models are widely used to explain the computation of a decision variable in the brain which reflects choice behaviour in two alternative task settings

(e.g. see Shadlen and Newsome (1996, 2001), Usher and McClelland (2001), Ditterich et al. (2003), Bogacz et al. (2006) and Teodorescu et al. (2016) for perceptual decisions, Krajbich et al. (2010, 2015), Basten et al. (2010) and Hunt et al. (2012) for value-based decisions, and Feng et al. (2009) and Afacan-Seref et al. (2018) where perceptual decisions are based on the integration of rewards associated with options presented). Although the stimulus implementation in our model-based analysis is primarily based on experimental and theoretical studies of perceptual decision-making (Teodorescu et al. 2016; Pirrone et al. 2018; Ratcliff et al. 2018), fluctuating stimuli have also been studied in other areas, such as collective behaviour of social insects (Franks et al. 2015; Hübner and Czaczkas 2017). Implementing the external stimulus as a periodic function with alternating low and high amplitudes, we have shown in our simulation analysis how the periodicity of a stimulus may be transduced to the dynamic evolution of the decision variable and the decision time distribution, which suggests that periodic stimuli may be used to modulate and shape behaviour.

The choice of the external stimuli and models applied in our simulations is motivated by previous model fitting analyses of experimental studies (Teodorescu et al. 2016; Ratcliff et al. 2018). In these studies, the brightness stimuli varied from frame to frame within each trial so that the resulting stimuli flickered (Teodorescu et al. 2016; Ratcliff et al. 2018). A corresponding model fitting analysis showed that whereas mDDM and LCA fit the data equally well in Teodorescu et al. (2016), Ratcliff et al. (2018) found in their study that mDDM fits explained the data better than LCA model fits. In the latter study, another DDM variant, which assumes that across-trial variability in drift rate scales with stimulus strength, performed equally well compared with the mDDM (Ratcliff et al. 2018). In both studies, fits of the standard DDM to the data were poor (Teodorescu et al. 2016; Ratcliff et al. 2018). Thus, we reasoned that the standard DDM is not suitable for our model analysis, and that the mDDM and a DDM where across-trial variability in drift rate varies with input magnitude would produce very similar behaviour. The comparison between mDDM and LCA, however, seemed interesting to us as in a previous study, both models performed equally well (Teodorescu et al. 2016) whereas in another (but similar) investigation, the mDDM performed better than the LCA (Ratcliff et al. 2018). Furthermore, we preferred a comparison between these two models because of the different properties and mechanics of mDDM (one-dimensional model, multiplicative noise) and those of the LCA (two-dimensional model, interacting accumulators). In our study, we nevertheless find that magnitude-sensitivity and frequency-sensitivity exhibited by mDDM and LCA are largely similar. The magnitude-sensitive results are in

agreement with those of (Teodorescu et al. 2016). Another influential sequential sampling model is the linear ballistic accumulator (LBA) (Brown and Heathcote 2008). However, in a classification of decision models (Teodorescu and Usher 2013), it has been shown that models with independent accumulators (such as the LBA) produce different behaviour than models featuring competition (such as the LCA). Based on these findings, we conjectured that the LBA model, although applicable to a wide range of perceptual decision-making tasks (Brown and Heathcote 2008), would not be suitable for the particular assumptions made in our study.

Intriguingly, our analysis reveals an interplay between the sensitivity of the model systems to frequency and magnitude of periodically applied stimuli. With regard to magnitude-sensitivity, our results (e.g. see Fig. 3 for continuous stimuli, and Figs. 4, 5, 6, 7, 8 and 9 for pulsed stimuli) are in line with previous findings (Pins and Bonnet 1996; Stafford and Gurney 2004; Palmer et al. 2005; Teodorescu et al. 2016; Pirrone et al. 2018; Hunt et al. 2012; Ratcliff et al. 2018; van Maanen et al. 2012; Reina et al. 2018). In particular, we observe a reduction of decision times with increasing overall magnitudes and magnitude ratios (in our study, the magnitude ratio was varied whilst the overall magnitude was kept constant which simultaneously changes the magnitude difference, cf. Table 2), as has been reported previously for perceptual decisions (Pins and Bonnet 1996; Stafford and Gurney 2004; Palmer et al. 2005; Teodorescu et al. 2016; Pirrone et al. 2018; Ratcliff et al. 2018; Polanía et al. 2014) and value-based decisions (Hunt et al. 2012; Pirrone et al. 2018; Polanía et al. 2014; Reina et al. 2018). Our simulations suggest that this magnitude-sensitive behaviour may additionally be shaped by frequency-sensitive effects which depend on frequency ratios, overall frequencies and the choice of the stimulus condition (see Figs. 4a, b, 5 and 6 for SC1, and 4c, d, 8 and 9 for SC2). In particular, we obtained equivalent effects under variation of magnitude ratios and frequency ratios when the pulsed stimulus has been applied under stimulus condition SC2 (Fig. 4c). Increasing either of the two ratios may increase evidence for one option, and therefore both quantities may act as modulators of decision-making in a similar way.

Empirical Evidence of Periodic Patterns in Reaction Time Distributions

Our finding that periodic stimuli may lead to periodicities in the distribution of decision times (Figs. 10 and 11) is a theoretical prediction of our model-based analysis. We are not aware of an empirical data set that has been obtained under conditions similar to those simulated in the present study and tests for such periodicities in reaction time distributions. However, in the context of rhythmic (or cyclic) perception, which is explained in more detail below,

periodicities in reaction time distributions are observed experimentally (e.g. see VanRullen and Dubois (2011) and VanRullen (2016) for summaries of related empirical observations). By making reference to empirical studies on cyclic perception, in the following, we argue why our predictions could possibly be also observed in suitably designed experiments, such as the one proposed in the “[Proposal of an Experimental Design](#)” section.

Rhythmic or cyclic perception indicates that cognition and perception involve sampling rhythms; that is, the probability to detect perceptual stimuli is not constant over time but rather oscillates with typical frequencies (VanRullen 2016). Regarding visual stimuli, for example, brain rhythmic activity for frequencies around 7 Hz (theta-band) and 11 Hz (alpha-band) have been linked to cyclic perception (VanRullen 2016). One possibility to think about rhythmically fluctuating perception is to consider perceptual thresholds being periodically modulated over time, as suggested by VanRullen (2016). This means that when the perceptual threshold alternates between lower and higher values, it is more likely that a perceptual stimulus which is integrated sequentially meets the threshold criterion when the oscillating perceptual threshold has momentary phase-dependent lower values (VanRullen 2016). Hence, the probability of perception will strongly depend on the phase of the stimulus presentation relative to the phase of the internal sampling rhythm of the brain.

Several more recent studies provide empirical evidence that rhythmic sampling is present in perception and cognition, such as the observation of theta-rhythmic reaction times in monkeys (Kienitz et al. 2018) and humans (Helfrich et al. 2018), and periodic detection accuracies in humans (Landau and Fries 2012; Fiebelkorn et al. 2013) under distributed attention when multiple stimuli are presented. Previously, periodic reaction time histograms with multiple equally spaced peaks have also been observed in visual pursuit movements (Latour 1967), in responses to acoustic clicks and light flashes (Harter and White 1968; White and Harter 1969) and in visual and auditory discrimination tasks (Dehaene 1993). From a more general point of view, although presented in the context of cyclic perception, these empirical findings provide strong evidence for the possibility of observing periodic patterns in reaction time distributions. Psychological data are however scarce, probably because of the challenges regarding the design of suitable experiments to enable the detection these periodicities (VanRullen and Dubois 2011).

To use the findings on rhythmic perception to interpret and support our results, we go back to the possible interpretation involving periodically fluctuating perceptual thresholds as introduced above. However, in our study, it is the perceptual stimulus that oscillates. Using periodic stimuli, evidence is presented with alternating high and low

intensities. Thus, we can assume that in the high-intensity phase, the decision variable experiences a steeper increase compared with the low-intensity stimulus phase. As we assumed a strong coupling between external stimulus and internal representation via Eq. 2, this suggests that the decision variable should increase rhythmically, i.e. a strong increase will be followed by a weak increase or decrease (depending on the information leak (as relevant in the LCA) and/or presentation of alternative stimuli (as relevant in the mDDM)) of the activity level, and so on. This should lead to a transduction of the period of the perceptual stimulus to the shape of the decision time distribution, which we observe in our simulation study (Figs. 10 and 11). Hence, it is the external frequency of the stimulus which should be obvious in the reaction time distribution, in contrast to the example with oscillating perceptual thresholds, where the internal frequency describing cyclic perception should be visible in the reaction time. However, in both cases (either oscillating perceptual stimuli or oscillating perceptual thresholds), the transfer of the frequency of the oscillating quantity to the reaction time distribution could apply in a similar way.

We point out that rhythmic sampling is not a model assumption in our study and that here the periodicity in the reaction time distribution most likely arises from the strong coupling of the perceptual stimulus to the decision variable via the psychophysical transfer function in Eq. 2. This means that in our study, cyclic perception can be assumed to be averaged out over the large number of trials, in which case our results do not depend on the presence or absence of rhythmic perception (i.e. the perceptual threshold may be assumed fixed rather than oscillating). Regarding the effects of periodic stimuli, it could also be the case that oscillating external input signals are smoothed when evidence is accumulated (Fig. 13), so that they are masked and not detectable in unsuitable experimental paradigms (or not detectable at all). Although our simulation results indicate the possibility that decision time distributions of real decision-makers responding to periodically oscillating stimuli might possibly show periodicities, whether or not our predictions hold in empirical data remains an open question. Finding a proper experimental set-up to test our predictions will therefore require more experimental and theoretical work to support or falsify our predictive theoretical study. Our proposal of a possible experimental approach discussed in the “[Proposal of an Experimental Design](#)” section may be a good starting point.

Supplementary Material Computer code for data generation and data analysis is open source and available under: <https://github.com/DiODE/Project/Frequency-sensitivity-and-magnitude-sensitivity-in-decision-making>.

Funding Information This work was funded by the European Research Council (ERC) under the European Union’s Horizon 2020 Research

and Innovation Programme (grant agreement number 647704). F.B. was funded by the SURE scheme of the University of Sheffield (UK).

Open Access This article is distributed under the terms of the Creative Commons Attribution 4.0 International License (<http://creativecommons.org/licenses/by/4.0/>), which permits unrestricted use, distribution, and reproduction in any medium, provided you give appropriate credit to the original author(s) and the source, provide a link to the Creative Commons license, and indicate if changes were made.

References

- Afacan-Seref, K., Steinemann, N.A., Blangero, A., Kelly, S.P. (2018). Dynamic interplay of value and sensory information in high-speed decision making. *Current Biology*, 28(5), 795–802.e6. <https://doi.org/10.1016/j.cub.2018.01.071>.
- Basten, U., Biele, G., Heekeren, H.R., Fiebach, C.J. (2010). How the brain integrates costs and benefits during decision making. *Proceedings of the National Academy of Sciences*, 107(50), 21767–21772. <https://doi.org/10.1073/pnas.0908104107>. <http://www.pnas.org/cgi/doi/10.1073/pnas.0908104107>.
- Bogacz, R., Brown, E., Moehlis, J., Holmes, P., Cohen, J.D. (2006). The physics of optimal decision making: A formal analysis of models of performance in two-alternative forced-choice tasks. *Psychology Review*, 113(4), 700–765. <https://doi.org/10.1037/0033-295X.113.4.700>. <http://doi.apa.org/getdoi.cfm?doi=10.1037/0033-295X.113.4.700>.
- Bogacz, R., Usher, M., Zhang, J., McClelland, J.L. (2007). Extending a biologically inspired model of choice: multi-alternatives, nonlinearity and value-based multidimensional choice. *Philosophical Transactions of the Royal Society B*, 362(1485), 1655–1670. <https://doi.org/10.1098/rstb.2007.2059>.
- Bose, T., Reina, A., Marshall, J.A. (2017). Collective decision-making. *Current Opinion in Behavioral Sciences*, 16, 30–34. <https://doi.org/10.1016/j.cobeha.2017.03.004>.
- Brown, E., & Holmes, P. (2001). Modeling a simple choice task: stochastic dynamics of mutually inhibitory neural groups. *Stochastics and Dynamics*, 1(02), 159–191. <https://doi.org/10.1142/S0219493701000102>.
- Brown, S.D., & Heathcote, A. (2008). The simplest complete model of choice response time: linear ballistic accumulation. *Cognitive Psychology*, 57(3), 153–178. <https://doi.org/10.1016/j.cogpsych.2007.12.002>. <https://www.sciencedirect.com/science/article/pii/S0010028507000722?via%3Dihub>.
- Brown, E., Gao, J., Holmes, P., Bogacz, R., Gilzenrat, M., Cohen, J.D. (2005). Simple neural networks that optimize decisions. *International Journal of Bifurcation and Chaos*, 15(03), 803–826. <https://doi.org/10.1142/S0218127405012478>.
- Brunton, B.W., Botvinick, M.M., Brody, C.D. (2013). Rats and humans can optimally accumulate evidence for decision-making. *Science*, 340(6128), 95–98. <https://doi.org/10.1126/science.1233912>.
- Dehaene, S. (1993). Temporal Oscillations in Human Perception. *Psychological Science*, 4(4), 264–270. <https://doi.org/10.1111/j.1467-9280.1993.tb00273.x>. <http://journals.sagepub.com/doi/10.1111/j.1467-9280.1993.tb00273.x>.
- Ditterich, J., Mazurek, M.E., Shadlen, M.N. (2003). Microstimulation of visual cortex affects the speed of perceptual decisions. *Nature Neuroscience*, 6(8), 891–898. <https://doi.org/10.1038/nn1094>. <http://www.nature.com/doi/10.1038/nn1094>; <http://www.nature.com/articles/nn1094>.
- Feng, S., Holmes, P., Rorie, A., Newsome, W.T. (2009). Can monkeys choose optimally when faced with noisy stimuli and

- unequal rewards? *PLoS Computational Biology*, 5(2), e1000284. <https://doi.org/10.1371/journal.pcbi.1000284>.
- Fiebelkorn, I., Saalman, Y., Kastner, S. (2013). Rhythmic sampling within and between objects despite sustained attention at a cued location. *Current Biology*, 23(24), 2553–2558. <https://doi.org/10.1016/J.CUB.2013.10.063>.
- Franks, N.R., Stuttard, J.P., Doran, C., Esposito, J.C., Master, M.C., Sendova-Franks, A.B., Masuda, N., Britton, N.F. (2015). How ants use quorum sensing to estimate the average quality of a fluctuating resource. *Scientific Reports*, 5(1), 11890. <https://doi.org/10.1038/srep11890>. <http://www.nature.com/articles/srep11890>.
- Gold, J.I., & Shadlen, M.N. (2007). The neural basis of decision making. *Annual Review of Neuroscience*, 30(1), 535–574. <https://doi.org/10.1146/annurev.neuro.29.051605.113038>.
- Harter, M.R., & White, C.T. (1968). Periodicity within reaction time distributions and electromyograms. *The Quarterly Journal of Experimental Psychology*, 20(2), 157–166. <https://doi.org/10.1080/14640746808400144>.
- Helfrich, R.F., Fiebelkorn, I.C., Szczepanski, S.M., Lin, J.J., Parvizi, J., Knight, R.T., Kastner, S. (2018). Neural mechanisms of sustained attention are rhythmic. *Neuron*, 99(4), 854–865.e5. <https://doi.org/10.1016/J.NEURON.2018.07.032>.
- Hübner, C., & Czaczkes, T.J. (2017). Risk preference during collective decision making: ant colonies make risk-indifferent collective choices. *Animal Behavior*, 132, 21–28. <https://doi.org/10.1016/j.anbehav.2017.08.003>.
- Hunt, L.T., Kolling, N., Soltani, A., Woolrich, M.W., Rushworth, M.F.S., Behrens, T.E.J. (2012). Mechanisms underlying cortical activity during value-guided choice. *Nature Neuroscience*, 15(3), 470–476. <https://doi.org/10.1038/nn.3017>.
- Kiebel, S.J., Daunizeau, J., Friston, K.J. (2008). A hierarchy of time-scales and the brain. *PLoS Computational Biology*, 4(11), e1000209. <https://doi.org/10.1371/journal.pcbi.1000209>.
- Kienitz, R., Schmiedt, J.T., Shapcott, K.A., Kouroupaki, K., Saunders, R.C., Christoph, M., Correspondence, S., Schmid, M.C. (2018). Theta rhythmic neuronal activity and reaction times arising from cortical receptive field interactions during distributed attention article theta rhythmic neuronal activity and reaction times arising from cortical receptive field interactions during distributed attention. *Current Biology*, 28, 2377–2387.e5. <https://doi.org/10.1016/j.cub.2018.05.086>.
- Krajbich, I., Armel, C., Rangel, A. (2010). Visual fixations and the computation and comparison of value in simple choice. *Nature Neuroscience*, 13(10), 1292–1298. <https://doi.org/10.1038/nn.2635>. <http://www.ncbi.nlm.nih.gov/pubmed/20835253>, <http://www.nature.com/articles/nn.2635>.
- Krajbich, I., Hare, T., Bartling, B., Morishima, Y., Fehr, E. (2015). A common mechanism underlying food choice and social decisions. *PLoS Computational Biology*, 11(10), e1004371. <https://doi.org/10.1371/journal.pcbi.1004371>. <http://www.econ.uzh.ch/faculty/fehr/>, <http://dx.plos.org/10.1371/journal.pcbi.1004371>.
- Landau, A., & Fries, P. (2012). Attention samples stimuli rhythmically. *Current Biology*, 22(11), 1000–1004. <https://doi.org/10.1016/J.CUB.2012.03.054>.
- Latour, P. (1967). Evidence of internal clocks in the human operator. *Acta Psychologica*, 27, 341–348. [https://doi.org/10.1016/0001-6918\(67\)90078-9](https://doi.org/10.1016/0001-6918(67)90078-9).
- Marshall, J.A.R., Favreau-Peigne, A., Fromhage, L., McNamara, J.M., Meah, L.F.S., Houston, A.I. (2015). Cross inhibition improves activity selection when switching incurs time costs. *Curr Zool*.
- Mauk, M.D., & Buonomano, D.V. (2004). The neural basis of temporal processing. *Annual Review of Neuroscience*, 27(1), 307–340. <https://doi.org/10.1146/annurev.neuro.27.070203.144247>.
- Pais, D., Hogan, P.M., Schlegel, T., Franks, N.R., Leonard, N.E., Marshall, J.A.R. (2013). A mechanism for value-sensitive decision-making. *PLoS ONE*, 8(9), e73216. <https://doi.org/10.1371/journal.pone.0073216>.
- Palmer, J., Huk, A.C., Shadlen, M.N. (2005). The effect of stimulus strength on the speed and accuracy of a perceptual decision. *Journal of Vision*, 5(5), 1. <https://doi.org/10.1167/5.5.1>.
- Pins, D., & Bonnet, C. (1996). On the relation between stimulus intensity and processing time: Piéron's law and choice reaction time. *Perception and Psychophysics*, 58(3), 390–400. <https://doi.org/10.3758/BF03206815>.
- Pirrone, A., Stafford, T., Marshall, J.A.R. (2014). When natural selection should optimize speed-accuracy trade-offs. *Frontiers in Neuroscience*, 8, 73. <https://doi.org/10.3389/fnins.2014.00073>.
- Pirrone, A., Azab, H., Hayden, B.Y., Stafford, T., Marshall, J.A.R. (2018). Evidence for the speed-value trade-off: human and monkey decision making is magnitude sensitive. *Decision*, 5, 129–142.
- Polanía, R., Krajbich, I., Grueschow, M., Ruff, C.C. (2014). Neural oscillations and synchronization differentially support evidence accumulation in perceptual and value-based decision making. *Neuron*, 82(3), 709–720. <https://doi.org/10.1016/j.neuron.2014.03.014>.
- Ratcliff, R. (1978). A theory of memory retrieval. *Psychology Review*, 85(2), 59–108. <https://doi.org/10.1037/0033-295X.85.2.59>. <http://content.apa.org/journals/rev/85/2/59>.
- Ratcliff, R., & Rouder, J.N. (1998). Modeling response times for decisions between two choices. *Psychological Science*, 9, 347–356.
- Ratcliff, R., & Tuerlinckx, F. (2002). Estimating parameters of the diffusion model: approaches to dealing with contaminant reaction times and parameter variability. *Psychonomic Bulletin and Review*, 9(3), 438–481. <https://doi.org/10.3758/BF03196302>.
- Ratcliff, R., Smith, P.L., Brown, S.D., McKoon, G. (2016). Diffusion decision model: current issues and history. *Trends in Cognitive Sciences*, 20(4), 260–281. <https://doi.org/10.1016/j.tics.2016.01.007>.
- Ratcliff, R., Voskuilen, C., Teodorescu, A. (2018). Modeling 2-alternative forced-choice tasks: accounting for both magnitude and difference effects. *Cognitive Psychology*, 103, 1–22. <https://doi.org/10.1016/j.cogpsych.2018.02.002>.
- Reina, A., Marshall, J.A.R., Trianni, V., Bose, T. (2017). Model of the best-of-*n* nest-site selection process in honeybees. *Physical Review E*, 95, 052411. <https://doi.org/10.1103/PhysRevE.95.052411>.
- Reina, A., Bose, T., Trianni, V., Marshall, J.A.R. (2018). Psychophysical laws and the superorganism. *Scientific Reports*, 8(1), 4387. <https://doi.org/10.1038/s41598-018-22616-y>. <http://www.nature.com/articles/s41598-018-22616-y>.
- Shadlen, M.N., & Newsome, W.T. (1996). Motion perception: seeing and deciding. *Proceedings of the National Academy of Sciences*, 93(2), 628–633. <https://doi.org/10.1073/pnas.93.2.628>. <http://www.pnas.org/cgi/doi/10.1073/pnas.93.2.628>.
- Shadlen, M., & Newsome, W. (2001). Neural basis of a perceptual decision in the parietal cortex (area LIP) of the rhesus monkey. *Journal of Neurophysiology*, 86(4), 1916–1936. <http://www.ncbi.nlm.nih.gov/pubmed/11600651>.
- Stafford, T., & Gurney, K.N. (2004). The role of response mechanisms in determining reaction time performance: Piéron's law revisited. *Psychonomic Bulletin & Review*, 11(6), 975–87. <https://doi.org/10.3758/BF03196729>. <http://www.ncbi.nlm.nih.gov/pubmed/15875968>, <http://www.springerlink.com/index/10.3758/BF03196729>.
- Sugrue, L.P., Corrado, G.S., Newsome, W.T. (2005). Choosing the greater of two goods: neural currencies for valuation and decision making. *Nature Reviews Neuroscience*, 6(5), 363–375.

- <https://doi.org/10.1038/nrn1666>. <http://www.nature.com/doi/finder/10.1038/nrn1666>, <http://www.nature.com/articles/nrn1666>.
- Tajima, S., Drugowitsch, J., Pouget, A. (2016). Optimal policy for value-based decision-making. *Nature Communications*, 7, 12400. <https://doi.org/10.1038/ncomms12400>. <http://www.nature.com/doi/finder/10.1038/ncomms12400>.
- Teodorescu, A.R., & Usher, M. (2013). Disentangling decision models: from independence to competition. *Psychology Review*, 120(1), 1–38. <https://doi.org/10.1037/a0030776>. <http://doi.apa.org/getdoi.cfm?doi=10.1037/a0030776>.
- Teodorescu, A.R., Moran, R., Usher, M. (2016). Absolutely relative or relatively absolute: violations of value invariance in human decision making. *Psychonomic Bulletin & Review*, 23(1), 22–38. <https://doi.org/10.3758/s13423-015-0858-8>. <http://link.springer.com/10.3758/s13423-015-0858-8>, <http://www.ncbi.nlm.nih.gov/pubmed/26022836>.
- Tye, K.M., & Deisseroth, K. (2012). Optogenetic investigation of neural circuits underlying brain disease in animal models. *Nature Reviews Neuroscience*, 13(4), 251–266. <https://doi.org/10.1038/nrn3171>. <http://www.nature.com/articles/nrn3171>.
- Usher, M., & McClelland, J.L. (2001). The time course of perceptual choice: the leaky, competing accumulator model. *Psychological Review*, 108, 550–592. <https://doi.org/10.1037/0033-295X.108.3.550>.
- van Maanen, L., Grasman, R.P.P.P., Forstmann, B.U., Wagenmakers, E.J. (2012). Piéron's Law and optimal behavior in perceptual decision-making. *Frontiers in Neuroscience*, 5, 143. <https://doi.org/10.3389/fnins.2011.00143>.
- VanRullen, R. (2016). Perceptual cycles. *Trends in Cognitive Sciences*, 20(10), 723–735. <https://doi.org/10.1016/j.tics.2016.07.006>.
- VanRullen, R., & Dubois, J. (2011). The psychophysics of brain rhythms. *Frontiers in Psychology*, 2, 203. <https://doi.org/10.3389/fpsyg.2011.00203>.
- Wald, A., & Wolfowitz, J. (1948). Optimum character of the sequential probability ratio test. *Annals of Mathematical Statistics*, 19(3), 326–339. <https://doi.org/10.1214/aoms/1177730197>. <http://projecteuclid.org/euclid.aoms/1177730197>.
- White, C.T., & Harter, M. (1969). Intermittency in reaction time and perception, and evoked response correlates of image quality. *Acta Psychologica*, 30, 368–377. [https://doi.org/10.1016/0001-6918\(69\)90060-2](https://doi.org/10.1016/0001-6918(69)90060-2).
- Wong, K.F., & Wang, X.J. (2006). A recurrent network mechanism of time integration in perceptual decisions. *Journal of Neuroscience*, 26(4), 1314–1328. <https://doi.org/10.1523/JNEUROSCI.3733-05.2006>.

Publisher's Note Springer Nature remains neutral with regard to jurisdictional claims in published maps and institutional affiliations.